Journal of Intelligent Manufacturing
https://doi.org/10.1007/s10845-026-02875-7

Model predictive force control in five-axis positional milling using a table dynamometer

Patrick Ochudlo[1] · Adrian Karl Rueppel[2] · Lorenz Schmidt[1] · Thomas Bergs[2] · Heike Vallery[1] · Sebastian Stemmler[1]

Received: 21 October 2025 / Accepted: 14 April 2026

Abstract

Milling is a highly flexible and productive machining process characterized by an intermittent tool-workpiece engagement. To further increase productivity, several force control strategies have been proposed to maintain a constant load on the milling tool for arbitrary engagement conditions. One example is model predictive force control (MPFC), which is attractive for milling because it achieves high control performance without requiring calibration experiments. However, so far it has been limited to three-axis milling. Machining processes for complex components like Blisks (bladed disks) require additional degrees of freedom, referred to as multi-axis synchronous milling. Multi-axis milling poses a sensing challenge: Table rotations disturb the force measurement of conventional table dynamometers. In this contribution, we propose an MPFC for five-axis positional milling (also referred to as 3+2-axis milling) as an intermediate step towards five-axis synchronous milling. We use an inverted measurement model to compensate for rotational disturbances and introduce a novel method to identify the angular position of the milling tool with maximum engagement for each position along the tool path in five-axis positional milling. Adaptations in the generation of the position-dependent reference and careful parameter tuning enable the control scheme to optimize the feed velocity without exceeding the computation time. The proposed method for approximating the maximum engagement is applicable to both three-axis and five-axis positional milling. In five-axis positional milling, it reduces the mean absolute force error from 42.6 N achieved with an established approximation to 1.2 N. In an experimental machining operation, the MPFC reduced machining time by 67 % compared with the manufacturer's recommended feed velocity, without substantially increasing the maximum tool load, and achieved a median absolute force-tracking deviation of only 10.3 N. Overall, these results demonstrate that the MPFC can be transferred from three-axis to five-axis positional milling while maintaining high control performance, representing an intermediate step towards application in five-axis synchronous milling.

Keywords Five-axis positional milling · Model predictive control · Table dynamometer · Force control · Engagement conditions

Introduction

Milling is a highly versatile machining process that is especially beneficial for manufacturing components with complex geometries and high quality requirements. The main influence on both component quality and production time is the process force that acts between the milling tool and the

✉ Patrick Ochudlo
p.ochudlo@irt.rwth-aachen.de

Adrian Karl Rueppel
adrian.rueppel@gmx.de

Lorenz Schmidt
lrnzschmidt@gmail.com

Thomas Bergs
t.bergs@mti.rwth-aachen.de

Heike Vallery
h.vallery@irt.rwth-aachen.de

Sebastian Stemmler
s.stemmler@irt.rwth-aachen.de

[1] Institute of Automatic Control, RWTH Aachen University, Campus-Boulevard 30, 52074 Aachen, NRW, Germany

[2] Manufacturing Technology Institute, RWTH Aachen University, Campus-Boulevard 30, 52074 Aachen, NRW, Germany

Published online: 22 May 2026

workpiece, which is monotonically related to the feed per tooth. For a constant spindle speed, the feed per tooth is proportional to the feed velocity, which is uncomplicated to manipulate in comparison to other machining parameters. Thus, feed velocity has become a key process variable in milling (Matsubara & Ibaraki, 2009). Very slow feed velocities keep tool loads low, but lead to extended production times. In contrast, inadequately high feed velocities cause excessive loads on the milling tool, and thus premature tool failure (Klocke, 2011, p. 345). Therefore, manipulating feed velocity as a function of process force is of great interest to improve milling processes (Ulsoy & Koren, 1993).

The process force depends strongly on the engagement conditions, which vary depending on the relative positions and respective geometries of both the milling tool and the workpiece. In particular, complex milling operations result in a wide range of engagement conditions and thus in varying process forces. Other factors such as tool wear and inhomogeneities in the workpiece material also substantially impact the process force (Klocke, 2011, pp. 68-71).

This high complexity poses challenges when introducing force control strategies in the milling process. Therefore, choosing a constant feed velocity that is tuned with respect to the worst-case engagement is often the most practical strategy in industrial milling. This leaves the potential of closed-loop force control largely unexploited, even though it could both increase productivity and reduce the dependence of process quality on operator experience (Ulsoy & Koren, 1993).

Motivated by this untapped potential, research has focused on force-based adaptation of feed velocity using various approaches. Early studies attempted to maintain a commanded active force using closed-loop control, namely fixed-gain controllers (Milner, 1974) and adaptive controllers (Lauderbaugh & Ulsoy, 1989; Ulsoy & Koren, 1989). Although promising results were reported when the cutting conditions matched those used during tuning, the need for reliable additional sensors and a narrow working range prevented the use of force control in industrial applications (Liang et al., 2004). A major step in realizing force control was the development of process simulation software, e.g., MasterCam or MACHpro, which has become industrially established (Altintas et al., 2014). These tools allow for the determination of engagement conditions along the tool path, and thus a sufficient prediction of process forces. Currently, popular approaches for force control can be divided into simulation-based open-loop control, referred to as feedrate scheduling (FS), and model-based closed-loop control (Matsubara & Ibaraki, 2009).

Because FS relies solely on simulation results, the calculated feed velocity can be executed on standard CNC machine tools without additional sensing, making the method attractive for industrial applications. The feed velocity is typically derived either from the material removal rate (MMR) or from mechanistic force models. MMR-based methods are easier to implement and thus already available in several commercial CAM systems. However, in complex three- to five-axis milling operations, only force model-based approaches currently achieve sufficient accuracy (Kurt & Bagci, 2011). Force model-based FS approaches invert a linear process model to compute the feed velocity needed to set commanded process forces. They obtain respective force model coefficients from calibration cuts (Boz et al., 2010; Erkorkmaz, 2013; Salami et al., 2007). Although these approaches provide excellent results immediately after calibration, the accuracy degrades continuously with progressive tool wear. The reason is the identified force model parameters, which do not adapt according to the tool wear. Consequently, FS approaches result in a mismatch between the active force in simulation and the milling operation, and thus in an increased load on the tool (Matsubara & Ibaraki, 2009). A promising solution is tool condition monitoring systems that detect tool wear and adapt the force model parameters accordingly (Liu et al., 2022). However, to the best of our knowledge, no tool condition monitoring system has been integrated in an FS approach to adapt the force model parameters and thus the feed velocity with respect to tool wear so far.

Closed-loop force control approaches, however, consider the changing process behavior inherently. In order to establish a closed-loop force control strategy in milling, various strategies have been explored to either measure or estimate the process force. Some estimate the process force based on motor currents (Altintas & Aslan, 2017; Tong et al., 2023) or accelerations (Bakhshandeh et al., 2024), while most control schemes rely on commercially available dynamometers (Altintaş, 1994; Altintas & Munasinghe, 1996; Koren, 1988; Lauderbaugh & Ulsoy, 1989).

Modern adaptive force control strategies optimize the feed velocity offline, similar to force model-based FS approaches. For force model parameter identification, calibration tests are conducted. An adaptive controller then adapts the feed velocity with respect to the commanded process force, with a safety margin that accounts for simulation inaccuracies (Altintas & Aslan, 2017; Nishida et al., 2019; Tong et al., 2023; Zuperl & Cus, 2012). These controllers were effective for arbitrary engagement conditions, although their effectiveness has so far been shown only for small errors in initially identified parameters, and their performance for greater identification deviations remains unknown. Moreover, the need for calibration experiments to identify the force model parameters complicates their use in industrial settings and therefore reduces their attractiveness for industrial applications.

Optimization-based control schemes with a continuously updated force model are particularly attractive for industrial use because they do not require such calibration for parameter identification. Our group previously proposed a model predictive force controller (MPFC) to adjust the feed velocity online, based on a prediction of the upcoming changes in the engagement conditions. In Schwenzer et al. (2022), we proposed a 2-layer design of the controller: A reference generator calculates a position-dependent trajectory of the feed velocity required to reach the commanded process force. The underlying process model is based on a nonlinear mechanistic force model and the engagement conditions acquired by simulation. The MPC transforms this position-dependent reference into a time-dependent one and sets the feed velocity, aiming for maximum productivity while not exceeding the reference velocity. Therefore, the MPC substantially increases the feed velocity while the milling tool is not engaged and sets it accordingly during engagement. To enable continuous adaptation, an ensemble Kalman filter (EnKF) identifies the force model parameters for the current revolution. Thus, the reference trajectory is generated based on the most recent force measurement. In addition, the EnKF enables identification in more complex engagement scenarios.

While the described MPFC showed good control performance in three-axis milling, the controller cannot be used in multi-axis milling. First, the influence of the machine table's rotation distorts the dynamometer-based measurement of process forces. Second, the controller approximates the maximum force per revolution based on the engagement conditions in the middle of the cutting depth, an approximation that is only valid in three-axis milling.

To overcome these limitations and make the MPFC applicable to five-axis positional milling, we extend the control algorithm described in Schwenzer et al. (2022) and make the following key contributions:

- Integrating a measurement model into the MPFC to reconstruct the process forces from table dynamometer measurements under arbitrary table orientations.
- Developing an approximation of the maximum force per revolution that enables online optimization of the feed velocity in multi-axis milling while accounting for varying engagement conditions along the tool's rotational axis.
- Demonstrating effective force control experimentally in five-axis positional milling.

Section Modeling presents the models and the force approximation necessary to apply the MPFC to multi-axis milling. The implementation of the main components is described in Section Model predictive force controller. Section Evaluation setup and protocol introduces the benchmark machining process and protocols for simulation and experiment. Section Results examines the approximation quality and the control performance. We discuss the performance of the MPFC and highlight the controller's potential for improvement in Section Discussion. Section Limitations focuses on limitations of the MPFC that are not yet addressed in its current version.

Modeling

Sections 3 introduce the submodels for a milling model in detail. Furthermore, Section Approximation of the maximum force per revolution presents a novel method to efficiently approximate the maximum force per revolution.

Model overview

The milling model for multi-axis milling consists of three submodels, shown in Fig. 1. The machine model approximates the dependency of the feed velocity v_{f} on the commanded feed velocity $v_{\mathrm{f,cmd}}$, based on the dynamics of the machine tool. The process model represents the engagement and therefore determines the process force F_{P} based on the feed velocity. In addition to the feed velocity, the process force depends on the engagement conditions between milling tool and workpiece. In multi-axis milling, the measured force is disturbed by the gravitational force F_{G} and oriented in the direction of the table dynamometer. Therefore, the measurement model describes the dependence of the measured force F_{M} on the process force F_{P} and other influences such as mass of the workpiece and orientation of the machine table. All three submodels are formulated to be computationally efficient for use in the MPFC. The computation time of each submodel remains below 1 ms per evaluation.

Machine model

The machine model approximates the three translational degrees of freedom of the machine tool with its built-in position and velocity control. Due to the impact of the underlying control loops on the dynamics of the machine tool, a modeling approach using a physics-driven model is not practical. Instead, the dynamics of the machine tool is modeled as a second-order lag system between the commanded feed velocity $v_{\mathrm{f,cmd}}$, which corresponds to the manipulated vari-

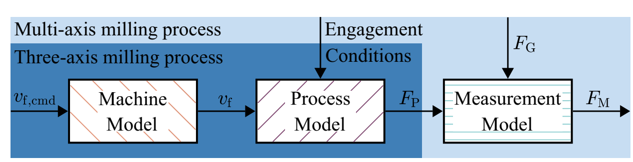

Fig. 1 Components of the model of a milling process according to Fussell and Srinivasan (1991). In the block diagram, we assume a constant spindle speed. The patterns represent the individual models and indicate which model is employed in each component of the control system

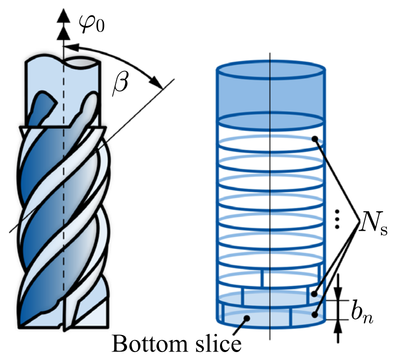

Fig. 2 Discretization of the milling tool according to Stemmler et al. (2019)

able, and the feed velocity v_f (Stemmler et al., 2017). Further details on the parametrization of the model and its quality can be found in Appendix A.

Process model

The process model describes how the process forces in tangential, radial, and passive directions depend on the feed velocity and various process parameters. We formulate a model based on the nonlinear Kienzle-model (Kienzle, 1952), combined with a runout model (Kline et al., 1982). In addition to the process parameters, the model comprises eight force model parameters, which are identified separately for each machining operation. The process model is defined and validated in detail in Rüppel et al. (2024). Therefore, we briefly summarize the key aspects relevant in this contribution below.

The Kienzle-model describes process forces according to the formation of chips, where chips are defined by their width b and thickness h. In addition to this geometric information, the Kienzle-model utilizes two empirical Kienzle-parameters k_i and m_i for each force direction to describe the milling process.

The Kienzle-model is applicable for a straight cutting edge. To account for the curved cutting edge of helical end mills with their helix angle β and number of teeth N_{th}, the milling tool is divided into N_{s} slices with the slice width b_n, as depicted in Fig. 2. The cutting edge for each slice is assumed to be straight, allowing the formulation of the Kienzle-model for each slice individually (Sutherland & DeVor, 1986). The discretization introduces several indices for force direction, tooth, tool slice, and discrete angular position, which are summarized in Table 1.

The angular position $\varphi_{q,n,j}$ is formulated for each slice n and each tooth j based on the angular position $\varphi_0(q)$ of the milling tool. Similarly, the force component $F_{i,n,j}$ according

Table 1 Explanation of the indices used in the process model

Index	Meaning	Range
i	force direction in CSCE	t (tangential), r (radial) and p (passive)
j	tooth index	$j \in [1, N_{\text{th}}]$
n	index of the slice in the discretized milling tool	$n \in [1, N_{\text{s}}]$
q	index of the discrete angular position of the bottom slice	$q \in [1, N_{\text{q}}]$

to the Kienzle-model is given by

$$F_{i,n,j} = k_i \delta(\varphi_{q,n,j}) b_n h_{q,n,j}^{1-m_i}, \; i \in \{t, r, p\} \tag{1}$$

for the process force in tangential (t), radial (r) and passive (p) directions, respectively. The overall force component is obtained by summing the contributions of all slices and teeth, reading:

$$F_i = \sum_{j=1}^{N_{\text{th}}} \sum_{n=1}^{N_{\text{s}}} F_{i,n,j}, \; i \in \{t, r, p\}. \tag{2}$$

The model depends on the angular position $\varphi_{q,n,j}$ of each cutting edge and the binary engagement factor δ, with

$$\delta(\varphi_{q,n,j}) = \begin{cases} 1 & \varphi_{\text{in},n} \leq \varphi_{q,n,j} \leq \varphi_{\text{ex},n} \\ 0 & \text{else} \end{cases}, \tag{3}$$

which indicates whether the angular position of the cutting edge is between the entry angle φ_{in} and the exit angle φ_{ex} with respect to tool and workpiece. The engagement of a slice is shown in Fig. 3.

Entry and exit angles, along with other geometric parameters such as the feed direction angle α and the cutting depth a_{p}, are obtained for discrete points on the tool path through an engagement simulation. They are summarized in the engagement condition matrix Ψ according to

$$\Psi = \left(\boldsymbol{p}_{\text{f}} \; \boldsymbol{\varphi}_{\text{in},1} \cdots \boldsymbol{\varphi}_{\text{in},\text{N}_\text{s}} \; \boldsymbol{\varphi}_{\text{ex},1} \cdots \boldsymbol{\varphi}_{\text{ex},\text{N}_\text{s}} \; \boldsymbol{\alpha} \; \boldsymbol{a}_{\text{p}} \cdots \right). \tag{4}$$

To acquire the engagement condition matrix, we use the software dPart (Ganser et al., 2021).

The chip thickness is composed of the undeformed chip thickness $h_{\text{nom},q,n,j}$ that forms during an ideal engagement of the milling tool, and the runout $h_{\text{rnt},n,j}$ that tool deflection causes. Hence, the chip thickness is defined as

$$h_{q,n,j} = h_{\text{nom},q,n,j} + h_{\text{rnt},n,j}(\rho_{\text{x}}, \rho_{\text{y}}, n, j, \beta, d_{\text{m}}, N_{\text{s}}). \tag{5}$$

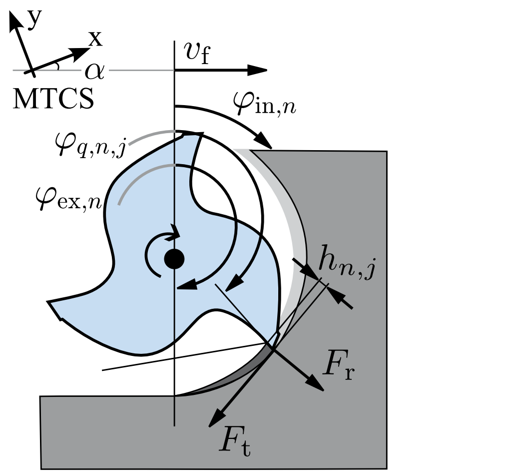

Fig. 3 Engagement of a single slice according to Stemmler (2020). MTCS denotes the machine tool coordinate system

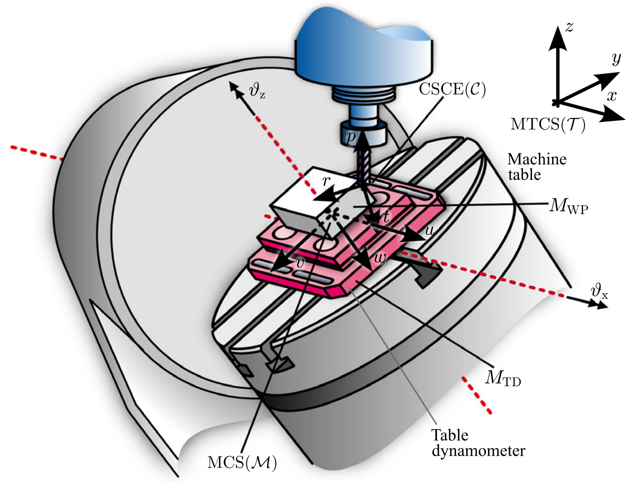

Fig. 4 Machine tool setup for multi-axis milling, highlighting the coordinate systems. The Machine Tool Coordinate System (MTCS) serves as the inertial coordinate system, the Measurement Coordinate System (MCS) is fixed to the table dynamometer, and the Coordinate System of the Cutting Edge (CSCE) is fixed to the milling tool

with the runout being dependent on tools diameter d_m, the helix angle β and the empirical runout parameters ρ_x and ρ_y. The undeformed chip thickness reads

$$h_{\mathrm{nom},q,n,j} = f_\mathrm{t}(v_\mathrm{f}, v_\mathrm{c}, d_\mathrm{nom}, N_\mathrm{th})|\sin\varphi_{q,n,j}| \tag{6}$$

with the cutting speed v_c. The functions are formulated in detail in Rüppel et al. (2024). In force control strategies, mainly the load on the milling tool perpendicular to its axis of rotation is of interest because these force components cause the deflection of the milling tool and, consequently, its breakage. This load is represented by the active force F_a, which is defined as

$$F_\mathrm{a} = \sqrt{F_\mathrm{t}^2 + F_\mathrm{r}^2}. \tag{7}$$

Measurement model

The measurement model describes the influence of the process force $\boldsymbol{F}_\mathrm{P}$ on the measured force $\boldsymbol{F}_\mathrm{M}$. It is formulated for a measurement setup with a table dynamometer mounted on a machine table, which has two rotational degrees of freedom, as depicted in Fig. 4. Conceptually, the model transforms the process force predicted in the coordinate system of the cutting edge (CSCE) into the machine tool coordinate system (MTCS), adds the gravitational force $\boldsymbol{F}_\mathrm{G}$ associated with the workpiece and measurement-related masses, and then transforms the resulting force into the measurement coordinate system (MCS)[1] of the dynamometer, taking into account the current table orientation and the tared gravitational load. The measurement model used in this contribution was first introduced and validated in Ochudlo et al. (2023) and is briefly summarized in the following.

The Kienzle-model defines the process force F_P in the coordinate system of the cutting edge (CSCE). the process force ${}^{\mathcal{C}}\boldsymbol{F}_\mathrm{P}$ reads

$${}^{\mathcal{C}}\boldsymbol{F}_\mathrm{P} = \left(F_\mathrm{t}\ F_\mathrm{r}\ F_\mathrm{p}\right)^\mathrm{T} \tag{8}$$

based on Eq. (2). The process force transforms into the MTCS according to

$${}^{\mathcal{T}}\boldsymbol{F}_\mathrm{P} = \left(F_\mathrm{x}\ F_\mathrm{y}\ F_\mathrm{z}\right)^\mathrm{T} = \sum_{j=1}^{N_\mathrm{th}} \sum_{n=1}^{N_\mathrm{s}} {}^{\mathcal{T}}\mathbf{C}_{\mathcal{C}}(\alpha, \varphi_{q,n,j})\, {}^{\mathcal{C}}\boldsymbol{F}_{\mathrm{P,n,j}} \tag{9}$$

with the rotation matrix ${}^{\mathcal{T}}\mathbf{C}_{\mathcal{C}}$ from CSCE to MTCS, which depends on the angular position $\varphi_{q,n,j}$ of the cutting edge and the feed direction angle α.

Besides the process force $\boldsymbol{F}_\mathrm{P}$, the gravitational force $\boldsymbol{F}_\mathrm{G}$ influences the measured force $\boldsymbol{F}_\mathrm{M}$. The dynamometer is tared before the machine table is rotated. Thus, an apparent constant negative force $-\boldsymbol{F}_{\mathrm{G},0}$ acts on the table dynamometer in the inverse orientation to where taring took place (frame $\mathcal{M}\simeq$). The gravitational effect depends on the workpiece mass M_WP and workpiece's initial mass $M_{\mathrm{WP},0}$, respectively. In MCS, the measured tared force ${}^{\mathcal{M}}\boldsymbol{F}_\mathrm{M}$ is expressed as

$$\begin{aligned} {}^{\mathcal{M}}\boldsymbol{F}_\mathrm{M} &= \left(F_\mathrm{u}\ F_\mathrm{v}\ F_\mathrm{w}\right)^\mathrm{T} \\ &= {}^{\mathcal{M}}\mathbf{C}_{\mathcal{M}_0}\, {}^{\mathcal{M}_0}\mathbf{C}_{\mathcal{T}}\left({}^{\mathcal{T}}\boldsymbol{F}_\mathrm{P} + {}^{\mathcal{T}}\boldsymbol{F}_\mathrm{G}(M_\mathrm{WP})\right) \\ &- {}^{\mathcal{M}_0}\mathbf{C}_{\mathcal{T}}\, {}^{\mathcal{T}}\boldsymbol{F}_{\mathrm{G},0}(M_{\mathrm{WP},0}) \end{aligned} \tag{10}$$

[1] The coordinate systems are represented as follows: a vector $\boldsymbol{a}$ is denoted as ${}^{\mathcal{C}}\boldsymbol{a}$ in the CSCE, ${}^{\mathcal{T}}\boldsymbol{a}$ in the MTCS and ${}^{\mathcal{M}}\boldsymbol{a}$ in the MCS.

with the constant rotation matrix ${}^{\mathcal{M}_0}\mathbf{C}_{\mathcal{T}}$ from MTCS to MCS at the instant of taring and the rotation matrix ${}^{\mathcal{M}}\mathbf{C}_{\mathcal{M}_0}$ that results from the machine table's nutation and spin angles about the x- and z-axes by angles ϑ_x and ϑ_z, respectively (precession angle is zero).

While the masses of the table dynamometer and the fixing aid remain constant during milling, material is continuously removed from the workpiece, decreasing the workpiece's initial mass. This continuously reduces the mass affecting the measurement. Thus, the material loss is calculated based on the prior work of Rüppel et al. (2023). The rotation matrices are provided in detail in Appendix B.

Approximation of the maximum force per revolution

Due to the intermittent engagement between workpiece and milling tool, the active force oscillates between its maximum and minimum level at tooth-passing frequency. This oscillation is irrelevant to the force controller, as the feed velocity is not intended to follow it. Instead, the controller considers the maximum active force $F_{\mathrm{a,max}}$ per revolution.

Since the active force depends on the orientation between milling tool and workpiece, the angular position φ_0 of the milling tool, depicted in Fig. 2, determines the maximum active force:

$$F_{\mathrm{a,max}} = F_\mathrm{a}(\varphi_{0,\max}),\ \text{where}\ \varphi_{0,\max} = \arg\max_{\varphi_0} F_\mathrm{a}(\varphi_0) \tag{11}$$

using the formulation in Eq. (7). The angular position $\varphi_{0,\max}$ denotes the angular position where the maximum active force over one revolution occurs.

Solving the optimization problem in Eq. (11) results in a high computation time. Since the controller operates at a high sampling rate, the optimization problem needs to be solved offline. Therefore, approximations of the maximum active force $F_{\mathrm{a,max}}$ are investigated to determine the corresponding angular position $\varphi_{0,\max}$.

According to (Schwenzer, 2022, p. 95), the maximum active force in three-axis milling occurs when the middle slice $\varphi_{q,\mathrm{N_s}/2,1}$ is perpendicular to the feed direction. When the middle slice is not engaged, the maximum active force occurs at the entry or exit angle of the tooth. Here, we refer to this approximation as the Approximation using the Middle Slice (AMS). It reads

$$\varphi_{0,\max} = \begin{cases} \varphi_\mathrm{in} + \Delta\varphi & , \varphi_\mathrm{in} \geq \frac{\pi}{2} - \Delta\varphi \\ \varphi_\mathrm{ex} & , \varphi_\mathrm{ex} \leq \frac{\pi}{2} + \Delta\varphi \\ \frac{\pi}{2} + \frac{\Delta\varphi}{2} & , \text{else} \end{cases} \tag{12}$$

with

$$\Delta\varphi = N_\mathrm{s} b_\mathrm{n} \frac{d_\mathrm{m}}{2} \tan(\beta). \tag{13}$$

AMS only holds when all slices along the tool's rotational axis have the same engagement conditions and when only one tooth is engaged at a time. In multi-axis milling, however, the tool's rotational axis is generally not aligned with the workpiece, resulting in different engagement conditions for each slice. To address this challenge, we propose a novel approximation strategy, which we refer to as Approximation using Convolution (AC).

To find the maximum active force over one revolution, the sum of the chip thicknesses needs to be maximized with respect to the engagement conditions. Because the force model parameters are unknown for a specific machining process, we seek a formulation that separates their influence from the engagement over one revolution. This separation enables computation of the angular position with maximum engagement offline, and online calculation of the active force by evaluating one angular position. For AC, we divide one revolution of the milling tool into N_q discrete angular positions, and thus the angular position φ_0 of the milling tool is described according to

$$\varphi_0(q) = (q-1)\frac{2\pi}{N_\mathrm{q}}. \tag{14}$$

The angular position $\varphi_{q,n,j}$ of each cutting edge depends on the angular position φ_0 of the milling tool, on the tooth j in relation to the number of teeth N_th and on the slice n taking into account the milling tool's shape (see Fig. 2):

$$\varphi_{q,n,j} = \varphi_0(q) - \frac{2(j-1)\pi}{N_\mathrm{th}} - \sum_{o=1}^{n}(o-0.5)b_n\frac{d_\mathrm{m}}{2}\tan(\beta). \tag{15}$$

The chip thickness consists of the undeformed chip thickness h_nom and the chip thickness h_rnt caused by runout (see Eq. (5). Since the runout parameters cannot easily be separated from the calculation of the chip thickness, we first examine the undeformed chip thickness h_nom according to Eq. (6) while neglecting runout. Neglecting the runout is possible because it is constant over one revolution for a given tooth and slice. The undeformed chip thickness depends on the feed velocity and the engagement conditions, and it is not directly influenced by the force model parameters. To find the maximum of the undeformed chip thickness, we introduce the engagement condition ψ per slice based on Eqs. (3-6), with

$$\psi(\varphi_{q,n,t}) = \delta(\varphi_{q,n,t})|\sin(\varphi_{q,n,t})|. \tag{16}$$

The cutting edges' angular positions are represented in the tool matrix $\mathbf{M}_\mathrm{tl} \in \mathbb{R}^{N_\mathrm{s} \times N_\mathrm{q}}$. This matrix stores the positions of the cutting edges around the circumference of the tool. Each row corresponds to a slice and each column to a discretized angular position. The entries of the tool matrix are 1 for the positions of the cutting edge and 0 for all other positions, resulting in a structure of the form

$$\mathbf{M}_{\text{tl}} = \begin{array}{c} \begin{pmatrix} 0\,1\,0 \dots 0\,0\,1\,0 \dots 0\,0\,0 \\ \vdots \\ 0\,0\,0 \dots 1\,0\,0\,0 \dots 0\,1\,0 \\ 0\,0\,0 \dots 0\,1\,0\,0 \dots 0\,0\,1 \end{pmatrix} \\ 2\pi \qquad \leftarrow \qquad 0 \end{array}. \tag{17}$$

The arrow below the matrix indicates the direction of an ascending angular position of the cutting edges.

The engagement conditions are represented by the engagement matrix $\mathbf{M}_\psi \in \mathbb{R}^{N_\text{s} \times N_\text{q}}$, which is defined as

$$\mathbf{M}_\psi = \begin{array}{c} \begin{pmatrix} \psi(\varphi_{1,N_\text{s},1}) & \dots & \psi(\varphi_{N_\text{q},N_\text{s},1}) \\ & \vdots & \\ \psi(\varphi_{1,1,1}) & \dots & \psi(\varphi_{N_\text{q},1,1}) \end{pmatrix} \\ 0 \qquad \rightarrow \qquad 2\pi \end{array} \tag{18}$$

By performing a convolution operation, denoted by $*$, between the tool and engagement matrices, we determine the angular position $\varphi_{0,\max}$ of the milling tool causing the maximum active force by evaluating the convolution result at angular index q and taking the column sum:

$$\varphi_{0,\max} = \varphi_0(q_{\max}), \qquad q_{\max} = \arg\max_q \left\| (\mathbf{M}_{\text{tl}} * \mathbf{M}_\psi)(q) \right\|_1 . \tag{19}$$

During convolution, each discrete angle in the tool matrix must match the corresponding discrete angle in the engagement matrix, so that the computed overlap represents the actual physical alignment. To compensate for the inherent inversion in the convolution operation, the order of ascending angular positions in the two matrices must be reversed, as already indicated in Eq. (17–18).

After computing the angular position with maximum undeformed chip thickness over one revolution (see Eq. (19), we consider the effect of runout, which affects the force on each tooth differently. Since runout depends on several process variables and may vary during machining, its effect is difficult to predict a priori. To account for the effect of runout without adding additional sensors for radial displacement, we compute the maximum active force by evaluating the active force for each tooth according to

$$F_{\text{a,max}} = \max_j F_a \left((\varphi_{0,\max} + (j-1) \frac{2\pi}{N_{\text{th}}}), v_\text{f} \right). \tag{20}$$

As the calculation is based on known runout parameters for a given feed velocity, it must be carried out online, resulting in N_th force evaluations, one for each tooth. Although the formulation does not reduce the online force evaluation to a single angular position per revolution, the number of evaluations remains acceptable for online computation of the maximum active force.

Model predictive force controller

The following sections introduce the closed-loop force controller and give details on the different components.

Controller overview

The above-mentioned models are employed in a model predictive force controller (MPFC), which is depicted in Fig. 5. The manipulated variable is the commanded feed velocity $v_\text{f,cmd}$, and the controlled variable is the active force F_a. The controller relies on the measurements of the feed position p_f, the feed velocity v_f, the angular position $\boldsymbol{\vartheta}$, and the measured force ${}^{\mathcal{M}}\boldsymbol{F}_\text{M}$. The measured force is transformed into the process force ${}^{\mathcal{T}}\boldsymbol{F}_\text{P}$ by inverting the rotation model in Eq. (10). The workpiece mass M_WP along the tool path is computed from the engagement condition matrix Ψ, which is obtained from an engagement simulation. While both the engagement condition matrix and the workpiece mass are computed a priori, the main components of the MPFC are repeatedly executed at every time step. Based on the engagement conditions and the measured process force, a parameter estimator identifies the state vector $\boldsymbol{x}_\text{PR}$ comprising the process force and the force model parameters. The updated force model parameters are then used by a reference generator to calculate the reference feed velocity $\boldsymbol{v}_\text{f,Ref}$ required to achieve the commanded active force $F_\text{a,cmd}$. Based on this velocity reference and the machine tool's state vector $\boldsymbol{x}_\text{MT}$, a velocity controller actuates the machine tool by setting the commanded feed velocity $v_\text{f,cmd}$. The machine tool's state vector $\boldsymbol{x}_\text{MT}$ is estimated using the Extended Kalman filter introduced in Stemmler (2020).

Although we do not explicitly evaluate the force-tracking error between commanded and measured active force, the measured process force is fed back in every time step through the online update of the process model. Since the measured process force includes the active force and directly influences the reference feed velocity, we classify the scheme as a closed-loop controller. In the following sections, the main components of the force control scheme are introduced in detail.

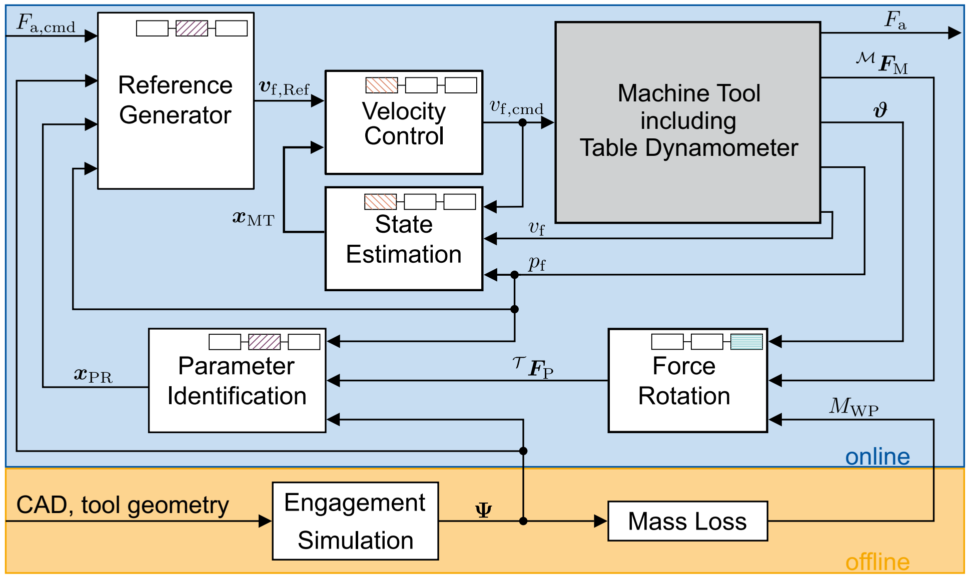

Fig. 5 Block diagram of the MPFC. The patterns indicate which models are used in the respective controller components (see Section Modeling)

Parameter estimation

Influencing factors like tool wear continuously change the dynamics of the milling process, leading to an increasing mismatch between the process forces predicted by the process model and those measured in machining. To adapt the process model to these varying dynamics, we continuously estimate the parameters of both the Kienzle-model and the runout model using an ensemble Kalman filter (EnKF) based on prior work of Schwenzer et al. (2022).

The state vector $\boldsymbol{x}_{\mathrm{PR}}$, which represents the milling process, contains the instantaneous process force in MTCS and the six force model parameters, resulting in

$$\boldsymbol{x}_{\mathrm{PR}} = \left(F_{\mathrm{x}}\ F_{\mathrm{y}}\ k_{\mathrm{t}}\ m_{\mathrm{t}}\ k_{\mathrm{r}}\ m_{\mathrm{r}}\ \rho_{\mathrm{x}}\ \rho_{\mathrm{y}}\right)^{\mathrm{T}}. \tag{21}$$

A detailed formulation of the EnKF can be found in Appendix C.

For tuning the EnKF, the number of particles N_{E} determines the ensemble size, and the measurement covariance $\boldsymbol{\Gamma}_{\mathrm{PR}}$ approximates the measurement noise. We assume that the influence of measurements in the x-direction on those in the y-direction, and vice versa, can be neglected. Thus, the measurement covariance $\boldsymbol{\Gamma}_{\mathrm{PR}}$ is a diagonal matrix, which reads

$$\boldsymbol{\Gamma}_{\mathrm{PR}} = \begin{pmatrix} \Gamma_{\mathrm{PR},1} & 0 \\ 0 & \Gamma_{\mathrm{PR},2} \end{pmatrix} \tag{22}$$

with the covariance values $\Gamma_{\mathrm{PR},1}$ and $\Gamma_{\mathrm{PR},2}$. The primary restriction on the number of particles is the sampling time. For initialization of the ensemble matrix $\mathbf{X}_{\mathrm{PR}}$, which comprises all particles, we used the approach introduced in Schwenzer et al. (2022). The force model parameters of different particles span over a wide range of materials, representing literature values from aluminum to Inconel and beyond. This approach guarantees convergence within the initial force model parameter space and eliminates the need for calibration experiments to roughly determine parameters for a specific machining process.

Reference generator

The reference generator calculates the reference feed velocity $v_{\mathrm{f,ref}}$ that results in the commanded active force $\boldsymbol{F}_{\mathrm{a,cmd}}$. The basic formulation of the reference generator used in this contribution was first introduced in (Schwenzer, 2022, pp.93-98). However, computational requirements required adaptations for multi-axis milling, as outlined in the following.

The reference generator calculates the reference dependent on the base position vector $\boldsymbol{p}_{\mathrm{f,Ref}}$. The base position vector comprises a number N_{Ref} of evenly spaced positions along the tool path, separated by the distance Δp_{f}, resulting in

$$\boldsymbol{p}_{\mathrm{f,Ref}}(k) = p_{\mathrm{f}}(k) + \left(0\ \Delta p_{\mathrm{f}}\ 2\Delta p_{\mathrm{f}}\ \ldots\ (N_{\mathrm{Ref}}-1)\Delta p_{\mathrm{f}}\right)^{\mathrm{T}}. \tag{23}$$

Due to the discretization of the milling tool, the reference feed velocity cannot be calculated analytically. Therefore, the reference generator solves the optimization problem

$$\min_{\boldsymbol{v}_{\mathrm{f,Ref}}} \left\| \boldsymbol{F}_{\mathrm{a,cmd}} - \boldsymbol{F}_{\mathrm{a,max}}(\varphi_{0,\max}(\boldsymbol{p}_{\mathrm{f,Ref}}), \boldsymbol{v}_{\mathrm{f,Ref}}, \mathbf{C}_{\mathrm{Ref}}\, \boldsymbol{x}_{\mathrm{PR}}) \right\|^2 \tag{24}$$

numerically using the derivative-free optimizer BOBYQA (Powell, 2009), considering the angular position $\varphi_{0,\max}$ with maximum engagement and the current force model parameters. For extracting the force model parameters from the parameter estimation state vector $\boldsymbol{x}_{\mathrm{PR}}$, we define the output matrix

$$\mathbf{C}_{\mathrm{Ref}} = \begin{pmatrix} \mathbf{0}_{2\times 2} & \mathbf{0}_{2\times 6} \\ \mathbf{0}_{6\times 2} & \mathbf{I}_{6\times 6} \end{pmatrix} \tag{25}$$

with the zero matrix $\mathbf{0}_{n\times m} \in \mathbb{R}^{n\times m}$ and the identity matrix $\mathbf{I}_{n\times n} \in \mathbb{R}^{n\times n}$.

In three-axis milling, the computational cost of determining the reference feed velocity was not a concern. Solving the optimization problem for $N_{\mathrm{Ref}} = 300$ base positions required approximately 22 ms in total (Schwenzer, 2022, p. 98). However, in multi-axis milling, the complex engagement conditions substantially increase the computation time per optimization. Solving the optimization problem for a single base position can take up to 4 ms, and the computation time is not deterministic. Consequently, in five-axis positional milling the reference generator can no longer compute the reference feed velocity for 300 base positions and requires modification. The modified working principle of the reference generator is shown in Fig. 6.

To reduce computational requirements, we increase the discretization distance to $\Delta p_{\mathrm{f}} = 0.3$ mm and interpolate values between two calculated references in increments of 0.05 mm to flatten the reference feed velocity. Since the reference generator determines the active force for the base position vector, the controller can respond only to changes in engagement conditions at the resolution provided by the discretization distance. Further increasing the discretization distance has proved impracticable because the controller can no longer accurately set the commanded feed velocity to prevent excessive force peaks. Despite these efficiency improvements, considering the worst-case calculation time, only five reference points are calculated per controller cycle, resulting in a reference feed velocity for only 1.5 mm ahead. This reference proved insufficient for the MPFC to adapt the

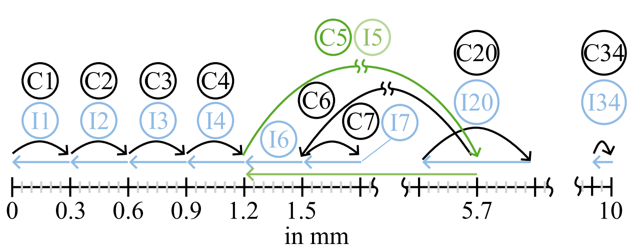

Fig. 6 Anticipatory operating principle of the reference generator with respect to abrupt changes in the engagement conditions. C marks positions at which the optimization explicitly computes a reference point. I marks positions filled in by linear interpolation

machine tool's feed velocity in time to react to abrupt changes in the engagement conditions.

Therefore, after four steps, the algorithm jumps ahead by 15 steps (or 4.5 mm) and linearly interpolates all values between these points. The machine tool needs roughly 10 ms to set large velocity differences, which occur for instance upon the tool's entry into the workpiece. Considering the maximum feed velocity, the machine tool would advance 1.9 mm in this time. In order to detect the entry into the workpiece early enough, a jump ahead in the reference of three times the maximum progress proved sufficient. This update strategy ensures that the MPFC always has sufficient, up-to-date information on the desired velocity. The optimization then resumes from step five (1.5 mm) until the next controller cycle begins. As a further precaution, the velocity vector is populated with the most recently calculated values up to a distance of 10 mm.

Velocity control

The reference generator computes a reference feed velocity that, according to the process model, results in the commanded active force. However, this computation does not take the machine tool's dynamic limitations into account. If the reference feed velocity were used directly as the manipulated variable, the limited acceleration and deceleration capabilities of the machine tool could lead to temporary force peaks, especially at abrupt changes in engagement conditions. The velocity control, therefore, aims to command the highest achievable feed velocity that does not violate the commanded force, while respecting the dynamic limitations of the machine tool. By predicting the near-future behavior of the machine tool and setting the manipulated variable at each time step k according to a cost function, the Model Predictive Controller (MPC) computes a commanded feed velocity that respects these dynamic limitations while staying as close as possible to the reference feed velocity. The MPC predicts the behavior over the prediction horizon, which is defined by the lower prediction horizon N_1 and the upper prediction horizon N_2. Predicted values over the prediction horizon are denoted as $(\cdot|k)$. By introducing the prediction horizon and minimizing a cost function for N_{u} optimization variables, the MPC handles the control task with respect to computational limits. The general formulation is introduced in detail in Maciejowski (2002). In this contribution, we use the reference-tracking linear MPC formulated in Stemmler et al. (2017).

Initially, the MPC transforms the position-dependent reference feed velocity into a time-dependent one. Based on the last predicted position $\boldsymbol{p}_{\mathrm{f}}(\cdot|k-1)$, the maximum possible increase in the current position is approximated by

$$\boldsymbol{p}_{\mathrm{f,max}}(\cdot|k) = \boldsymbol{p}_{\mathrm{f}}(\cdot|k-1) + T_{\mathrm{s}} v_{\mathrm{f,cmd,max}} \tag{26}$$

with the maximum feed velocity $v_{\mathrm{f,cmd,max}}$ that the machine tool can safely provide. The maximum feed velocity $v_{\mathrm{f,max}}$ is determined according to

$$\boldsymbol{v}_{\mathrm{f,max}}(\cdot|k) = \boldsymbol{v}_{\mathrm{f,Ref}}\left(\boldsymbol{p}_{\mathrm{f}}(\cdot|k-1)\right) \tag{27}$$

based on the prediction of the MPC and the reference feed velocity calculated by the reference generator. Formulating the optimization problem requires decomposing the commanded feed velocity $v_{\mathrm{f,cmd}}(k)$ into the previously commanded velocity $v_{\mathrm{f,cmd}}(k-1)$, which cannot be further optimized, and the optimized commanded velocity $\Delta v_{\mathrm{f,cmd}}(\cdot|k)$ according to

$$\boldsymbol{v}_{\mathrm{f,cmd}}(\cdot|k) = v_{\mathrm{f,cmd}}(k-1) + \begin{pmatrix} 1 & \cdots & 0 \\ \vdots & \ddots & \vdots \\ 1 & \cdots & 1 \end{pmatrix} \Delta\boldsymbol{v}_{\mathrm{f,cmd}}(\cdot|k). \tag{28}$$

The MPC determines the position and velocity over the prediction horizon using the state space defined in Eq. (D15), which enables the MPC to predict the position $\boldsymbol{p}_{\mathrm{f}}(\cdot|k)$ and velocity $\boldsymbol{v}_{\mathrm{f}}(\cdot|k)$ using both the known future system dynamics and the dynamics caused by changes in the commanded feed velocity. The prediction is introduced in detail in Appendix D.

The cost function for the MPC consists of four terms: the tracking error between the desired and predicted positions, the change in the optimized variable, and two terms minimizing the slack variable ε, which introduces soft constraints on the feed velocity. These terms are weighted by the weighting matrices $\mathbf{Q}$, $\mathbf{R}$, and $\mathbf{T}$, respectively:

$$\begin{aligned} \min_{\Delta\boldsymbol{v}_{\mathrm{f,cmd}},\boldsymbol{\varepsilon}} & \|\boldsymbol{p}_{\mathrm{f,max}}(\cdot|k) - \boldsymbol{p}_{\mathrm{f}}(\cdot|k)\|_{\mathbf{Q}}^2 + \|\Delta\boldsymbol{v}_{\mathrm{f,cmd}}(\cdot|k)\|_{\mathbf{R}}^2 \\ & + \|\boldsymbol{\varepsilon}(\cdot|k)\|_{\mathbf{T}}^2 + \mathbf{T}\boldsymbol{\varepsilon}(\cdot|k). \end{aligned} \tag{29}$$

For the weighting matrices, we choose

$$\mathbf{Q} = \mathbf{I}, \qquad \mathbf{R} = \gamma\mathbf{I}, \quad \mathbf{T} = \eta\mathbf{I}, \tag{30}$$

with the tuning parameters γ and η. The optimization is subject to constraints

$$\begin{aligned} \boldsymbol{v}_{\mathrm{f,cmd}}(\cdot|k) &\leq \boldsymbol{v}_{\mathrm{f,cmd,max}}, \\ \boldsymbol{v}_{\mathrm{f}}(\cdot|k) &\leq \boldsymbol{v}_{\mathrm{f,max}}(\cdot|k) + \boldsymbol{\varepsilon}(\cdot|k), \\ \boldsymbol{\varepsilon}(\cdot|k) &\geq \mathbf{0}, \end{aligned} \tag{31}$$

which encode that the commanded feed velocity may not exceed the maximum velocity of the machine tool, and that the feed velocity may not exceed the velocity given by the reference generator. The non-negative slack variable $\boldsymbol{\varepsilon}$ is introduced to guarantee feasibility at each time step when the second constraint cannot be satisfied.

Optimization is carried out using the solver qpKWIK, which is provided by Schmid and Biegler (1994). Although optimization considers the commanded feed velocity over the entire prediction horizon, the MPC only outputs the current commanded feed velocity $v_{\mathrm{f,cmd}}(k|k)$ to actuate the machine.

Evaluation setup and protocol

For evaluation of the MPFC, we designed a test geometry and defined appropriate production parameters for stable machining, presented in Section 4.1. Section 4.2 explains the simulative validation of the approximation of the engagement conditions in detail. Additionally, we conducted experiments on a specialized machine tool integrating a non-industrial hardware framework, which allowed acquisition of detailed signals and precise manipulation of the machining process, as described in Section 4.3.

Design of the benchmark machining process

The benchmark five-axis positional machining process used in this work was first introduced in Rüppel et al. (2024) and is briefly described here. The machined geometry, depicted in Fig. 7, was designed to cover a wide range of engagement conditions that are typical in industrial milling processes. Consequently, tuning the algorithm to a particular engagement scenario was not possible.

In both three-axis milling and five-axis positional milling, the milling tool enters and exits the workpiece three times. The first cut (area **A**) is characterized by a straight entry and an exit with an angle of 32° with the tool engaged with its full diameter in the workpiece. In the second cut (area **B**), the milling tool enters the workpiece with an angle of 32° and exits the workpiece straight. The milling tool has a radial immersion of 75 % of the tool diameter. In the third cut (area **C**), characterized by a greater cutting depth, both entry and exit are straight, and the milling tool has a radial immersion of half its diameter.

In three-axis milling, the milling tool and workpiece are aligned ($\vartheta_{\mathrm{x}} = 0°$), whereas in five-axis positional milling, the workpiece is tilted by $\vartheta_{\mathrm{x}} = 20°$ during machining. Tilting the workpiece increases process complexity, because the engagement conditions vary along the tool height from slice to slice, while in three-axis milling they remain identical for all slices at each position on the tool path (see Fig. 8).

Particularly during the quick entry and exit of the milling tool, rapid changes in the engagement conditions highlight the force controller's ability to suppress force peaks. In contrast, the constant engagement phases reveal the overall control performance and adaptability under uniform conditions.

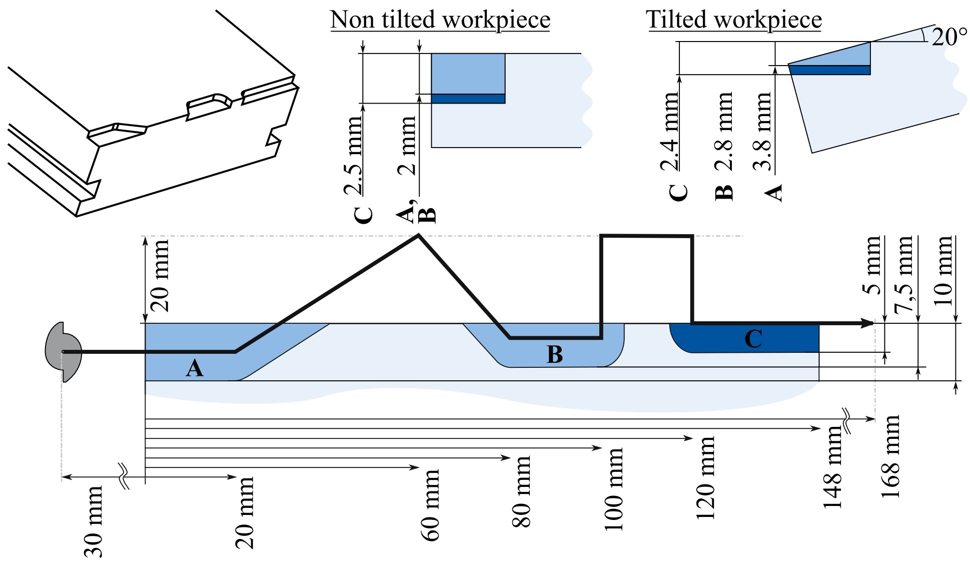

Fig. 7 Detailed representation of the machined geometry with its three cuts A–C according to Rüppel et al. (2024)

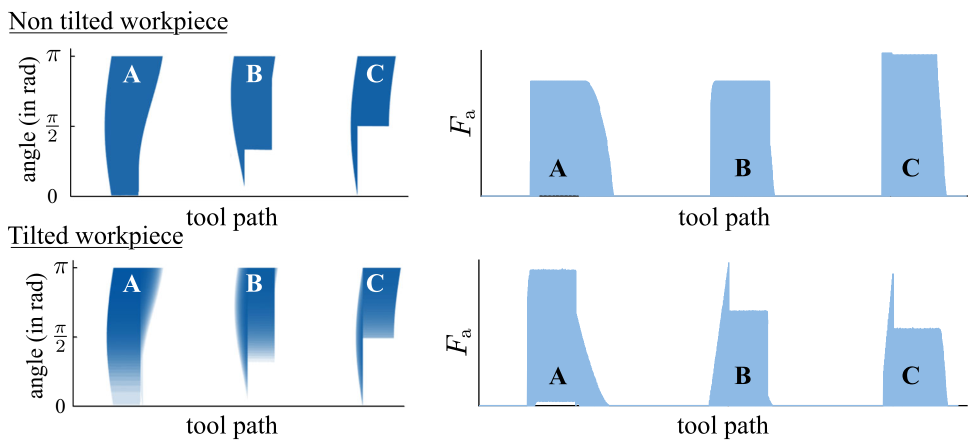

Fig. 8 Left: Engagement region between entry and exit angles in which slices are engaged. A more intense color indicates a higher number of engaged slices. Right: Qualitative representation of the expected active force when machining the test geometry at a constant feed velocity

To visualize these effects, Fig. 8 additionally shows the qualitative active force that occurs in simulation when machining with a constant feed velocity for both three-axis and five-axis positional milling.

As discussed, the active force comprises both quick changes and constant sections. The increased complexity in multi-axis milling is especially notable during the tool's entry and exit, where the engagement conditions change for each position on the milling path and for each slice differently, resulting in a more complex shape of the active force.

We set up the milling process according to the manufacturer's recommendations and pre-trial results. The process parameters are shown in Table 2.

Simulation protocol to validate the approximation of the maximum force per revolution

The approximation of the maximum force per revolution is a key factor to enable online optimization of the feed velocity with respect to the predicted active force. The AMS has already proven to be applicable in three-axis milling.

We hypothesize that the AC provides similar quality in approximating the maximum force in three-axis milling as the AMS. Furthermore, we expect AC to maintain high approximation quality in multi-axis milling.

To validate the approximations, we performed simulations of the milling process for both three-axis and five-axis positional milling using the simulation model introduced in Rüppel et al. (2024).

The force was calculated with a sample rate of 5 kHz to ensure that the active force is computed close to its peak. To obtain the maximum active force per revolution, we introduced a sliding window spanning one revolution. The maximum active force inside the sliding window was determined, then the window advanced forward by one revolution, resulting in non-overlapping segments covering the entire simulation result.

For each sample point where a maximum active force was found, the active force was also calculated using the same

Table 2 Parameters of the machining process

Number of teeth N_{th} (-)	Tool diameter d_m (in mm)	Helix angle β (in °)	Cutting speed v_c (in m min^{-1})	Slice width b_n (in mm)
2	10	35	80	0.1

Table 3 Force model parameters in simulation

Kienzle-parameters				Run-out parameters	
k_t (in N/mm^2)	k_r (in N/mm^2)	m_t (-)	m_r (-)	ρ_x (in mm)	ρ_y (in mm)
1720	122	0.17	0.61	−0.001	−0.001

process parameters and $\varphi_{0,\max}$ from both AMS and AC. As quality metrics, the mean absolute error (MAE) and the maximum difference $\Delta F_{a,\max}$ between the maximum simulated active force[2] and the approximation were determined. The maximum difference $\Delta F_{a,\max}$ reads

$$\Delta F_{a,\max} = F_{a,\max}(\varphi_{0,\max}) - \overline{F}_{a,\max}, \tag{32}$$

We conducted each simulation using a constant feed velocity, ensuring that process force variations arose solely from changes in the engagement conditions.

To choose the feed velocity appropriately, we relied on information provided by the tool manufacturer. The tool manufacturer provides recommendations for the feed velocity based on the workpiece material and the engagement conditions. For a fully engaged milling tool with a cutting depth of 2.5 mm and 42CrMo4 as a workpiece material, the manufacturer recommends a feed velocity between a minimum of $v_{f,\min} = 7.64\,\text{mm}\,\text{min}^{-1}$ and a maximum of $v_{f,\max} = 183.35\,\text{mm}\,\text{min}^{-1}$ (Seco Tools GmbH, 2025). Thus, we performed simulations considering these two technological limits and their resulting mean value. We used the same feed velocities for both three-axis milling and five-axis positional milling because the manufacturer did not provide recommendations for a multi-axis milling process.

The force model parameters set in the simulation are shown in Table 3.

Experimental protocol to validate the mpfc

The effectiveness of force controllers can be demonstrated by their ability to maintain a commanded force throughout the machining process and maximize the feed velocity when not engaged. The general effectiveness of an MPFC has already been shown for three-axis milling by Schwenzer et al. (2022).

We hypothesize that our proposed MPFC can similarly maintain the commanded active force in five-axis positional milling, thereby significantly reducing production time compared to machining with a constant feed velocity, without adversely affecting the milling tool. We expect our proposed controller to achieve similar results in five-axis positional milling as the force controller introduced by Schwenzer et al. (2022) in three-axis milling.

To validate the MPFC, we manufactured the geometry introduced in Section 4.1 three times. We conducted machining operations on a five-axis Mazak VARIAXIS i-600 machine tool equipped with a Siemens SINUMERIK 840D sl numerical control (NC) unit. The workpiece material was 42CrMo4 steel, and the milling tool was the two-fluted cemented carbide end mill JSE512100D2C.0Z2 SIRA supplied by Seco Tools GmbH, Erkrath, Germany. The initial workpiece mass was 8.78 kg for the controlled experiment and 8.14 kg for the experiment with constant feed velocity, respectively. During machining, 7 g of workpiece material is removed from the workpiece.

A measurement setup comprising a Kistler 9255B table dynamometer, connected to a Kistler charge amplifier Type 5070, recorded the forces at a sampling rate of 5 kHz, i.e., about 60 times higher than the tooth-passing frequency of 85 Hz. The controller ran on a compact Rio (cRio) real-time edge computer by National Instruments with a sampling rate of 50 Hz. Process signals were obtained via the Axis Data Stream (ADAS) software feature and transmitted at 500 Hz to the cRio device. To manipulate the feed override, the cRio communicated with the NC via OPC Unified Architecture (OPC UA). The override was updated via synchronous function.

Preliminary tests were performed to determine appropriate parameters for the force controller. The corresponding parameters are summarized in Table 4. Both the MPC and the EnKF were configured such that their computations are always completed within one control cycle. In terms of control effectiveness, the tests revealed that the choice of the MPFC parameters γ and N_2 most substantially affects control performance. Consequently, the parameter tuning focused particularly on these two parameters.

Since closed-loop force control in multi-axis milling is currently an active research topic, a technological and economic view on choosing the optimal commanded active force in multi-axis milling has been lacking thus far. Therefore, we determined an appropriate commanded active force based

[2] To distinguish between measurement and model-based calculation of a variable a, we denote the measured variable as $\overline{a}$.

Table 4 Parameters of the MPFC in the experimental validation

EnKF tuning parameters		MPC tuning parameters								
$\Gamma_{\mathrm{PR},1}$ (-)	$\Gamma_{\mathrm{PR},2}$ (-)	N_1 (-)	N_u (-)	N_2 (-)	η (-)	γ (-)	N_E (-)	N_Ref (-)	T_s (in s)	$v_{\mathrm{f,cmd,max}}$ (in mm min^{-1})
3000	3000	3	4	16	10^4	0.5	20	200	0.02	1272

on the tool manufacturer's information for three-axis milling provided in Section 4.2.

Hence, we machined the non-tilted geometry in Fig. 7 using the recommended maximum feed velocity $v_\mathrm{f} = 183.35\,\mathrm{mm\,min^{-1}}$. The maximum active force measured in this experiment was 342.3 N. Since we used a new tool, the tool manufacturer guarantees safe operation of the milling tool for forces below this value. Therefore, we set the commanded active force to $F_{\mathrm{a,cmd}} = 300\,\mathrm{N}$ for the closed-loop experiments with a tilted workpiece. For the baseline experiment, we again chose the tool manufacturer's recommended maximum feed velocity.

We evaluated the force controller's performance using multiple quality metrics. Since the controller's objective is to maximize productivity, we consider the overall machining time and the cutting time, where the tool is actively engaged. The latter metric is particularly relevant because it remains unaffected by the feed velocity between cuts, which might be carefully adjusted in industrial applications. However, this adjustments would require the use of simulation tools that are not always available in industry, or a trial-and-error approach that requires substantial time and operator experience, making the adaptation attractive only for long production times or high-volume manufacturing.

Besides maximizing productivity, maintaining a desired commanded force is a main concern for the force controller. Preliminary evaluations revealed that evaluating the difference between commanded and measured active forces throughout the machining process is heavily influenced by limitations in machine dynamics and inaccuracies in the simulated engagement conditions. These effects overshadowed the exceeding of the commanded active force, which is the key factor in maintaining the force. Thus, force metrics comprising the entire machining process provide limited insight into the controller's effectiveness.

To capture short but potentially tool-damaging peaks in the active force, we evaluate the maximum active force $\|F_\mathrm{a}\|_\infty$ during machining. As a measure of the force-tracking performance, we introduce the median absolute deviation (MAD), which quantifies the deviation from the commanded force while being robust to the aforementioned limitations. To further focus on exceedances of the commanded active force, we compute the root mean square error for all N_cg instances where the active force exceeds the commanded active force, indicated as CG-RMSE in the following. The CG-RMSE reads

$$\text{CG-RMSE} = \sqrt{\frac{1}{N_\mathrm{cg}}\sum_{i=1}^{N_\mathrm{cg}}(F_{\mathrm{a},i} - F_{\mathrm{a,cmd}})^2}, \text{ where } F_{\mathrm{a},i} > F_{\mathrm{a,cmd}}. \tag{33}$$

Results

We conducted both simulations and milling experiments to evaluate approximation quality and force controller performance. In the following sections, we present these results.

Simulation results

The simulated active force and the calculated active force based on both approximations for three-axis and five-axis positional milling are shown in Fig. 9. Circles indicate the maximum simulated active force in each segment of the sliding window.

The performance of the approximations is summarized in Table 5. Overall, as the feed velocity increased, the maximum active force as well as the MAE and the maximum deviation tended to increase for both approximations. A notable exception was the MAE for small feed velocities using AC in five-axis positional milling, which is higher compared to the MAE for increased feed velocities.

For three-axis milling, both approximations performed equally well, with MAE values below 1 N for all feed velocities. The AC proved less susceptible to temporary inaccuracies, reducing the maximum deviation to 29.5 N compared to 64.0 N for the AMS.

By contrast, the AMS no longer accurately represented the maximum force per revolution in five-axis positional milling, resulting in an increase in MAE of up to 42.6 N. In comparison, the AC maintained an MAE of 1.24 N, thereby outperforming the AMS.

Experimental results

An exemplary result of the five-axis positional milling experiment with the tool manufacturer's recommended feed velocity and with the closed-loop manipulated feed velocity

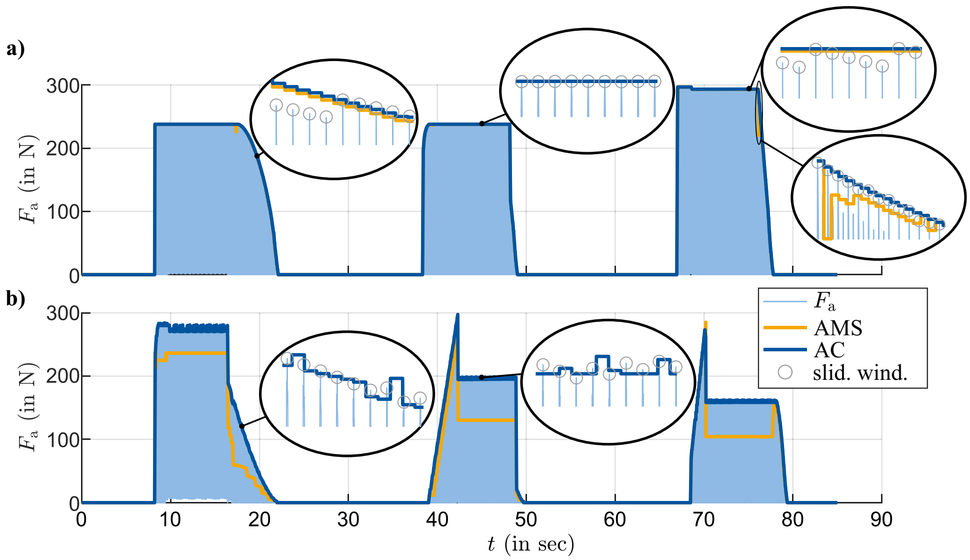

Fig. 9 Simulated active force from the process model and corresponding approximations of the maximum active force during machining of the test geometry at a constant feed velocity of 183.35 mm min^{-1}, **a)** for a non-tilted workpiece, **b)** for a tilted workpiece. AMS refers to the established Approximation using the Middle Slice, whereas AC denotes the Approximation using Convolution (see Section Approximation of the maximum force per revolution). The label slid. wind. refers to the sliding window, which is used to determine the maximum active force per revolution. The figure shows that both the AMS and the AC correctly determine the angular position at which the maximum force per revolution occurs. While the AMS can no longer approximate the maximum active force per revolution in five-axis positional milling, the AC still maintains a high approximation quality

Table 5 Comparison of the approximation quality for different feed velocities

	feed velocity v_f (in mm min^{-1})	max.force $\|F_a\|_\infty$ (in N)	quality metric AMS MAE (in N)	max. force difference $\|\Delta F_{a,max}\|_\infty$ (in N)	quality metric AC MAE (in N)	max. force difference $\|\Delta F_{a,max}\|_\infty$ (in N)
Three-axis	7.64	54.34	0.0955	13.2	0.0852	5.05
	95.5	185.6	0.439	41.8	0.479	6.04
	183.35	296.6	0.790	64.0	0.872	29.5
Five-axis position.	7.64	64.97	17.0	34.7	5.98	13.6
	95.5	186.5	28.7	68.6	1.22	27.4
	183.35	297.1	42.6	103	1.24	24.5

is depicted in Fig. 10 and Fig. 11, respectively. The maximum active force obtained from the sliding window is shown in blue, and the predicted maximum active force based on the identified force model parameters is shown in green.

The results of the five-axis positional milling experiments are summarized in Table 6. When manufacturing with the constant feed velocity, the active force remained below the commanded value for most of the machining operation, resulting in a maximum peak force of 322 N and a CG-RMSE of 6.53 N. However, the good performance in avoiding force exceedance came at the expense of poor force-tracking performance. The constant feed velocity led to a conservative active force for most of the machining process (see Fig.10), as reflected by a MAD of 89.7 N and a machining time of 86.1 s.

In contrast, the MPFC achieved substantially better force-tracking performance with a MAD of 10.3 N, and thereby reduced the machining time to 28.6 s (corresponding to a time reduction of approximately 67 %). Exceedances of the commanded force occurred more frequently, however, the MPFC was able to prevent high peak forces, limiting the maximum peak force to 384 N and the CG-RMSE to 26.1 N (see Fig. 11).

To put our results in perspective, we additionally evaluated both the time and force metrics from the three-axis milling experiment in Schwenzer et al. (2022). In that study, the commanded active force was increased to 500 N because

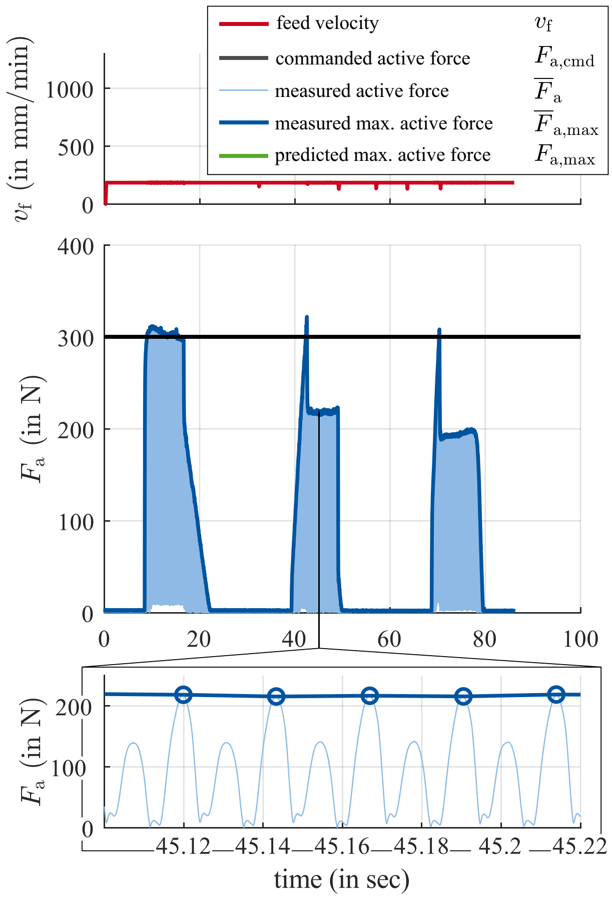

Fig. 10 Feed velocity and resulting active force in baseline experiment, where a constant feed velocity of 183.35 mm min^{-1} was used

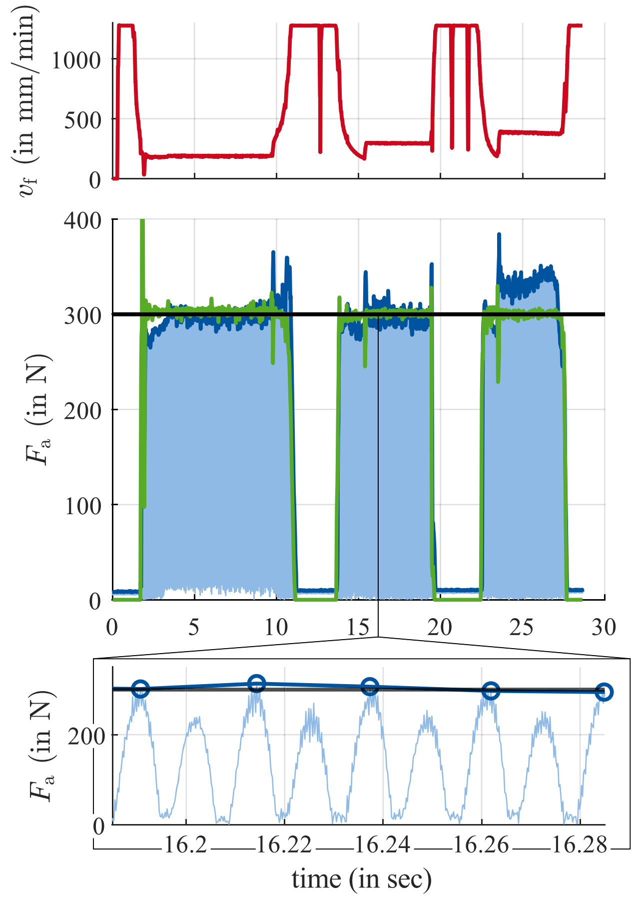

Fig. 11 Feed velocity and resulting active force using the MPFC. The figure shows the controller's ability to maintain the active force at its commanded value during machining of the test geometry by adjusting the feed velocity

the workpiece material and therefore the tool manufacturer's recommendation differed. Furthermore, the constant feed velocity was set less conservatively, resulting in a higher force-tracking performance, but at the same time in higher force exceedance and thus in a CG-RMSE of 60.6 N instead of 6.53 N as observed in this contribution.

The MPFC improved maintaining the commanded force compared to machining with a constant feed velocity, reducing both the MAD from 37.8 N to 22.0 N and the CG-RMSE from 60.6 N to 13.5 N. Since reducing active force exceedance resulted in similar cutting times, the controller reduced the machining time mainly by increasing the feed velocity between cuts (Schwenzer et al., 2022).

Discussion

The following sections evaluate and discuss both the approximation quality and the controller performance.

Quality of the approximation of the maximum force per revolution

In three-axis milling, the low MAE indicated that both the AMS and the AC generally determined the correct angular position $\varphi_{0,\max}$, where the maximum active force per revolution occurred (see Table 5). The MAE was similar for both approximation methods, and the AC was more robust against temporary approximation errors of the engagement conditions, which was shown by the reduced maximum deviation.

Hence, our hypothesis was confirmed that the AC provides a high approximation quality in three-axis milling. Since the AMS has already demonstrated its effectiveness in a closed-loop force controller, the similarly performing AC can probably be used in three-axis milling without decreasing control performance. The smaller maximum deviation may reduce the likelihood of high peak forces, but was not verified in this contribution.

Table 6 Results of the experimental validation in five-axis positional milling and experimental validation from Schwenzer et al. (2022) in three-axis milling for comparison

	commanded force $F_{\mathrm{a,cmd}}$ (in N)	force metric MAD (in N)	CG-RMSE (in N)	max. force $\|F_{\mathrm{a}}\|_{\infty}$ (in N)	cutting time t_{cut} (in sec)	machining time t_{total} (in sec)
		Five-axis positional milling				
MPFC	300	10.3	26.1	384	20.6	28.6
Const. feed velocity	300	89.7	6.5	322	35.2	86.1
		Three-axis milling (from Schwenzer et al. (2022))				
MPFC	500	22.0	13.5	529	25.3	33.6
Const. feed velocity	500	37.8	60.6	626	25.5	63.6

Inaccuracies in the approximation can be separated into two categories. The first category was the model error due to approximation inaccuracies, particularly noticeable when engagement conditions changed rapidly, as exemplarily observed in Fig. 9 a) at 76.1 s using the AMS.

The second type was a periodic deviation between the simulation and the approximation, which arose from discrete sampling of the angular position in simulation. If the angular position was not sampled exactly at the point of the highest active force, a small error occurred because the approximation suggested a slightly higher active force than the simulation. We provide a more detailed analysis of this deviation in Appendix E. This deviation became more severe with smaller tool engagements, especially observable at the tool exit and in the third cut.

We were unable to separate these two types of errors without increasing the sample rate of the simulation model, which, however, is not possible in the experimental validation due to the sampling rate of the table dynamometer. Consequently, we did not compensate for the periodic deviation, but rather evaluated the combined resulting error.

In five-axis positional milling, the AMS no longer accurately determined the maximum force, causing the MAE to increase to 42.6 N. The different engagement conditions across the milling tool's height probably prevented an accurate approximation using the middle slice.

In contrast, the AC maintained good model quality for a wide range of feed velocities, achieving a MAE of less than 1.24 N for high feed velocities. Inaccuracies arising from the sampling rate of the simulation model likely accounted mainly for the observed deviation. Furthermore, minor fluctuations in the engagement conditions acquired by the engagement simulation reduced the approximation accuracy. Thus, we could confirm our hypothesis that the AC is both viable in three-axis and five-axis positional milling.

Further improving approximation quality would require an increase in the number of slices N_{s}. However, a trade-off between accuracy and calculation time needs to be found to operate the MPFC. For small feed velocities, numerical inaccuracies had a greater impact on the model quality, resulting in an MAE of 5.98 N for the minimum feed velocity. For the machining process in this contribution, however, a high feed velocity was desired and, therefore, the lower technological limit of the feed velocity was less critical. The MAE of less than 1.24 N for higher feed velocities and a maximum deviation comparable to that of the AMS in three-axis milling indicate that the AC has a high approximation quality and can be used in an MPFC for five-axis positional milling.

It is important to note that the evaluation of the active force at all angular positions unlike $\varphi_{0,\max}$ led to lower active forces than the true maximum active force. However, in the open-loop simulation, the feed velocity was not adjusted based on this incorrect approximation. Using an incorrect approximation in a closed-loop experiment would result in high oscillations of the active force due to inaccurate identification and prediction of the active force, potentially leading to the controller becoming unstable. This could result in damaging the machine tool, therefore, we do not test an MPFC including the AMS in five-axis positional milling in this contribution.

Performance of the force controller

The experiments indicate that the MPFC is able to maintain a commanded active force in a five-axis positional milling operation, clearly outperforming the machining approach using a constant feed velocity. The MPFC reduced the MAD from 89.7 N in the experiment with a constant feed velocity to 10.3 N, while maintaining the commanded active force with just minor force exceedance and a CG-RMSE of 26.1 N (see Table 6). Considering this CG-RMSE and the overall maximum active force of 384 N across all three experiments, it is highly unlikely that the process forces adversely affected the milling tool. Thus, our hypothesis that the MPFC is applicable in five-axis positional milling is confirmed.

High peak forces in the controlled experiment were primarily observed when the engagement conditions changed rapidly. Presumably, the MPFC could not fully compensate for these changes due to model inaccuracies. Nevertheless, the controller quickly adapted to maintain the commanded active force, thereby limiting excessive process forces. Under steady engagement conditions, the controller effectively maintained the commanded active force with only minor inaccuracies, most likely due to slight mismatches in the force model parameters or small errors induced by the measurement model.

At the beginning of the first cut, the EnKF caused a decrease in the commanded velocity. While converging to an accurate set of force model parameters, the parameters temporarily represented higher process forces than experimentally observed, forcing the reference generator to calculate a commanded feed velocity smaller than actually needed. This slowing effect is visible at 1.8 s in the peak of the predicted active force shown in Fig. 11. We could have improved the prediction of the active force if we had initialized the force model parameters in a smaller range typical for the workpiece material. However, since the ensemble converged to a realistic set of parameters after only a few iterations, we decided to preserve the wide initial range to ensure convergence for different materials without tuning.

Identification quality decreased with increasing cutting depth, as observed in the third cut starting at 23.3 s. Since the MPFC comprises a force model-based optimization and velocity controller, feed velocity adaptations are not directly driven by the difference between commanded and measured active forces, but rather by the difference between commanded and predicted values based on the force model parameters identified. Consequently, high identification quality is essential for good control performance.

When investigating identification quality more thoroughly, high peak forces caused by the non-converged estimation overshadowed other inaccuracies in the identification. Thus, we excluded predicted peak active forces that were more than twice the control goal from the evaluation. After removing these large outliers, the CG-RMSE of the calculated active force above the commanded active force was only 8.7 N and therefore substantially lower than the CG-RMSE of the measurement. Assuming a perfect identification, the CG-RMSE using the predicted active force would closely match the CG-RMSE considering the measured active force. Thus, CG-RMSE indicates that there remains potential to improve the identification of force model parameters.

The machining time revealed the major benefit of the MPFC, as it enabled a reduction of 67 % in production time compared to the constant feed velocity. This reduction can be explained by two effects: First, the machine tool increases the feed velocity when the milling tool is not engaged, thereby shortening the time spent outside the workpiece. In the baseline experiment, the feed velocity remained constant between engagements. As discussed in Section 4.3, this part of the machining process could be improved in industrial applications, albeit with considerable additional effort. Second, the MPFC reduces the cutting time t_{cut} from 35.2 s to 20.6 s. This reduction is the result of optimization of the feed velocity with respect to the current active force, which is only possible using a force controller. Consequently, production time can be reduced by at least 41 %, even if the feed velocity between engagements is already optimized via other means.

Comparing our proposed MPFC with the one presented in Schwenzer et al. (2022) is challenging because of differences in the workpiece material and commanded velocity. The authors in Schwenzer et al. (2022) focused on the reduction of process force exceedance. Thus, the cutting time remained constant, and the controller achieved a reduction in production time only by increasing the feed velocity between cuts compared to their benchmark test. While our MPFC achieved a smaller MAD in five-axis positional milling, the CG-RMSE and maximum active force for five-axis positional milling both surpassed values for three-axis machining in Schwenzer et al. (2022). However, all values are in a comparable range. Thus, our results support the hypothesis that our MPFC performs comparably in five-axis positional milling as the controller in Schwenzer et al. (2022) in three-axis milling despite the additional complexity. However, for a detailed analysis of the control performance, both controllers should be evaluated under identical conditions, which is not part of this contribution.

The results demonstrate that the introduced test geometry (see Fig. 7) enables a detailed analysis of the force-tracking performance of the controllers. With a maximum active force of 322 N in the experiment using a constant feed velocity, our choice of a commanded force of 300 N was appropriate. However, the test geometry only partially allows validation of the compensation for gravitational effects in the force measurement. The gravitational force $\|{}^{\mathcal{M}}F_{\mathrm{G}}\|$ affects the measurement in u-direction by approximately 99 N in the controlled experiment, i.e., about one third of the commanded force. Therefore, the initial workpiece mass and the table alignment are well suited to validate the correct integration of the force rotation model. In contrast, the removed workpiece mass of 7 g changes the measured force by only about 0.02 N during machining. Consequently, the integration of the mass loss model cannot be substantially validated by machining the test geometry in this work.

In addition to validation of the mass loss model, longer machining times would result in progressive tool wear, which is a major challenge for modern control schemes. From a theoretical point of view, the MPFC should be able to compensate for tool wear by continuously adapting the force model parameters to the current tool state. This, however, still needs to be demonstrated in future experiments. In our current setup, substantially extending the machining time was not possible due to limitations in the microcontroller's memory and, consequently, in the maximum tool path length.

Limitations

Although the control scheme demonstrates that advanced control methods are applicable to milling, its current implementation is confined to rough milling with end mills and depends on force measurements from a table dynamometer.

While primarily focusing on process forces acting on the milling tool is sufficient in rough milling, geometric tolerances and surface quality become dominant performance criteria in finishing operations. The MPFC shows potential to effectively satisfy geometric tolerances by maintaining the active force at a commanded level. Thus, tool deflection is limited and becomes more uniform throughout machining, which, in combination with appropriately chosen commanded forces, can potentially result in reduced scrap. However, the controller currently adapts the feed velocity very frequently. In turning, frequent variations of the feed velocity are known to promote favorable chip breakage, but this oscillation must be chosen carefully in order to maintain a high surface quality (Smith et al., 2010). Before using the MPFC in finishing operations, additional constraints on manipulating the feed velocity will likely need to be included in the control law to achieve a high surface quality.

Beyond end mills, the MPFC framework could also be adapted to other tool geometries by modifying the process model and the engagement simulation, utilizing engagement models for ball end mills (Lee & Altintaş, 1996) or new tool shapes such as barrel end mills (Olvera et al., 2020). Additionally, more complex tool path planning strategies could be added to the reference generator, which account for effects such as tool deflection (López de Lacalle et al., 2007). However, all of these extensions must be implemented with respect to the limited computation time, as additional geometric computations will increase the computational complexity.

As long as motor current-based force estimation lacks sufficient accuracy for online force model parameter identification, the control scheme must rely on additional sensors. Novel sensor systems such as rotating cutting dynamometers (Kuljanic et al., 2002) or sensory-tool holders (Möhring et al., 2020; Schuster et al., 2023) are unaffected by gravitational and inertial effects, eliminating the need to compensate for these effects. However, their acceptance and widespread integration in industrial milling remain uncertain.

Conclusion

In this contribution, we adapted an MPFC for five-axis positional milling.

Experimental results confirmed that the controller effectively handled the increased complexity of five-axis positional milling. It maintained the commanded active force across various engagement conditions and prevented high peak forces, thereby ensuring a safe machining process. As the controller design is path-independent, only the results from the engagement simulation have to be updated for different milling operations.

Further research will extend the validation to industrial machining processes that involve substantial material removal, greater cutting depths, and application of coolant. Such machining operations will indicate the influence of the mass loss model on the control performance and test the controller under progressive tool wear.

Our experimental results have already revealed a gradual loss of performance at greater cutting depths. Most likely, the EnKF and reference generator cause this gradual performance loss, since they would exceed their maximum allowable sample times without the adaptations and careful tuning emphasized in this publication. Although the limited computation time of the reference generator did not appear to impact control performance in our experiments, a decrease in control performance was observed due to an inaccurate identification of force model parameters, probably caused by a poor discretization in the parameter estimation. Consequently, reducing the computation time is a key factor in further improving the MPFC.

When extending the MPFC for five-axis synchronous milling, the inertial forces acting on the table dynamometer have to be compensated for, and the enlarged engagement table has to be adapted for use on real-time hardware. Apart from that, no structural changes to the force controller are required.

Appendix A Details on the machine model

The transfer function of the machine tool relating the commanded feed velocity $v_{\mathrm{f,cmd}}$ to the resulting feed velocity v_{f} reads

$$\frac{V_{\mathrm{f}}(s)}{V_{\mathrm{f,cmd}}(s)} = \frac{K\omega_0^2}{s^2 + 2\zeta\omega_0 s + \omega_0^2}\mathrm{e}^{-sT_{\mathrm{d}}} \tag{A1}$$

Table 7 Parameters of the machine model

Static gain K (-)	Damping ζ (-)	Cutoff-frequency ω_0 (in s^{-1})	Time delay T_d (in s)
1	1	100	0.04

with the static gain K, the damping ratio ζ, the cutoff frequency ω_0, the time delay T_d, and the Laplace variable s.

The numerical values of the model parameters are given in Table 7. We identified them based on step responses that represent a wide range of velocity changes, which occur regularly in milling. Identification was carried out using the Matlab Identification Toolbox (Rüppel et al., 2024). The resulting model reproduces the experimental data with a normalized root mean square error of 6.46 %.

Appendix B Details on the measurement model

The rotation matrix ${}^{\mathcal{T}}\mathbf{C}_{\mathcal{C}}$ from CSCE to MTCS depends on the angular position $\varphi_{q,n,j}$ of the cutting edge and the feed direction angle α:

$$
{}^{\mathcal{T}}\mathbf{C}_{\mathcal{C}} = \begin{pmatrix} \cos(\alpha - \varphi_{q,n,j}) & -\sin(\alpha - \varphi_{q,n,j}) & 0 \\ \sin(\alpha - \varphi_{q,n,j}) & \cos(\alpha - \varphi_{q,n,j}) & 0 \\ 0 & 0 & 1 \end{pmatrix}. \tag{B2}
$$

The constant rotation matrix ${}^{\mathcal{M}_0}\mathbf{C}_{\mathcal{T}}$ from MTCS to MCS at the instant of taring and the rotation matrix ${}^{\mathcal{M}}\mathbf{C}_{\mathcal{M}_0}$ that results from the machine table's nutation and spin angles about the x- and z-axes by angles ϑ_x and ϑ_z, respectively (precession angle is zero), read:

$$
\begin{aligned}
{}^{\mathcal{M}}\mathbf{C}_{\mathcal{M}_0} &= \begin{pmatrix} \cos(\vartheta_\mathrm{z}) & -\sin(\vartheta_\mathrm{z}) & 0 \\ \sin(\vartheta_\mathrm{z}) & \cos(\vartheta_\mathrm{z}) & 0 \\ 0 & 0 & 1 \end{pmatrix} \begin{pmatrix} 1 & 0 & 0 \\ 0 & \cos(\vartheta_\mathrm{x}) & -\sin(\vartheta_\mathrm{x}) \\ 0 & \sin(\vartheta_\mathrm{x}) & \cos(\vartheta_\mathrm{x}) \end{pmatrix}, \\
{}^{\mathcal{M}_0}\mathbf{C}_{\mathcal{T}} &= \begin{pmatrix} 1 & 0 & 0 \\ 0 & -1 & 0 \\ 0 & 0 & -1 \end{pmatrix}.
\end{aligned} \tag{B3}
$$

Appendix C Details on parameter estimation

The EnKF estimates the states in two steps, including a model-based propagation and a correction using current measurements. To propagate the ensemble, we introduce the ensemble matrix $\mathbf{X}_\mathrm{PR}$,

$$
\mathbf{X}_\mathrm{PR} = \left(\boldsymbol{x}_{\mathrm{PR},1} \ \ldots \ \boldsymbol{x}_{\mathrm{PR},N_\mathrm{E}}\right), \tag{C4}
$$

with the number of particles N_E for propagation. Each particle $\tilde{\boldsymbol{x}}_{\mathrm{PR},i}(k)$ is propagated under the assumption that the force model parameters remain constant from the last update. Based on these updated force model parameters, the process force in MTCS is calculated, and each particle $\tilde{\boldsymbol{x}}_{\mathrm{PR},i}$ is propagated according to

$$
\begin{aligned}
&\tilde{\boldsymbol{x}}_{\mathrm{PR},i}(k) \\
&= \left(F_\mathrm{x}\left(\hat{\boldsymbol{x}}_{\mathrm{PR},i}(k-1), v_\mathrm{f}(k)\right) \ F_\mathrm{y}\left(\hat{\boldsymbol{x}}_{\mathrm{PR},i}(k-1), v_\mathrm{f}(k)\right) \ \hat{\boldsymbol{x}}^\mathrm{T}_{\mathrm{PR},i}(k-1)\right)^\mathrm{T}
\end{aligned} \tag{C5}
$$

using the process model described in Section Process model. The state covariance $\mathbf{P}_\mathrm{PR}$ is determined by calculating the variance of the propagated particles, which reads

$$
\mathbf{P}_\mathrm{PR} = \frac{1}{N_\mathrm{E}} \left(\tilde{\mathbf{X}}_\mathrm{PR}(k) - E(\tilde{\mathbf{X}}_\mathrm{PR}(k))\right) \left(\tilde{\mathbf{X}}_\mathrm{PR}(k) - E(\tilde{\mathbf{X}}_\mathrm{PR}(k))\right)^\mathrm{T}. \tag{C6}
$$

The correction step is based on the force measurement obtained by the table dynamometer. The measurement vector $\boldsymbol{y}_\mathrm{PR}$ is defined as

$$
\boldsymbol{y}_\mathrm{PR} = \mathbf{C}_\mathrm{PR}\boldsymbol{x}_\mathrm{PR}, \tag{C7}
$$

where the process output matrix $\mathbf{C}_\mathrm{PR}$ is given by

$$
\mathbf{C}_\mathrm{PR} = \begin{pmatrix} 1 & 0 & 0 & 0 & 0 & 0 & 0 & 0 \\ 0 & 1 & 0 & 0 & 0 & 0 & 0 & 0 \end{pmatrix}. \tag{C8}
$$

To account for measurement noise, the measurement covariance $\boldsymbol{\Gamma}_\mathrm{PR}$ is defined, and noise samples η_i are extracted according to

$$
\eta_i \sim \mathcal{N}(\mathbf{0}, \boldsymbol{\Gamma}_\mathrm{PR}), \tag{C9}
$$

where the noise values of all samples represent white Gaussian noise. The perturbed measurement z_i is obtained by adding the noise value η_i to the measurement $\overline{\boldsymbol{y}}_\mathrm{PR}$ according to

$$
z_i(k) = \overline{\boldsymbol{y}}_\mathrm{PR}(k) + \boldsymbol{\eta}_i(k). \tag{C10}
$$

Analogous to the ensemble matrix, the noise matrix $\mathbf{E}$ defined as

$$
\mathbf{E}(k) = \left(\boldsymbol{\eta}_1(k) \ \cdots \ \boldsymbol{\eta}_{N_\mathrm{E}}(k)\right) \tag{C11}
$$

is introduced. Based on this formulation, the approximated measurement covariance matrix $\mathbf{R}_\mathrm{PR}$ reads

$$
\mathbf{R}_\mathrm{PR}(k) = \frac{1}{N_\mathrm{E}}\mathbf{E}(k)\mathbf{E}^\mathrm{T}(k). \tag{C12}
$$

The Kalman gain $\mathbf{K}_{\mathrm{PR}}$, which weights the measurement and the propagation, is computed according to

$$\mathbf{K}_{\mathrm{PR}}(k) = \mathbf{P}_{\mathrm{PR}}(k)\mathbf{C}_{\mathrm{PR}}^{\mathrm{T}} \left(\mathbf{C}_{\mathrm{PR}}\mathbf{P}_{\mathrm{PR}}(k)\mathbf{C}_{\mathrm{PR}}^{\mathrm{T}} + \mathbf{R}_{\mathrm{PR}}(k)\right)^{-1} \tag{C13}$$

and the state vector updated as follows

$$\hat{\mathbf{x}}_{\mathrm{PR},i}(k) = \tilde{\boldsymbol{x}}_{\mathrm{PR},i}(k) + \mathbf{K}_{\mathrm{PR}}(k)\left(z_i(k) - \mathbf{C}_{\mathrm{PR}}\tilde{\boldsymbol{x}}_{\mathrm{PR},i}(k)\right). \tag{C14}$$

Appendix D Details on velocity control

To derive the MPC, the machine model's transfer function in Eq. (A1) is transformed into a state-space representation. The state vector $\boldsymbol{x}_{\mathrm{MT}}$ of the machine tool comprises the position p_{f} on the tool path, the feed velocity v_{f} and the feed acceleration $\dot{v}_{\mathrm{f}}$. Considering the input u_{MT}, the output vector $\boldsymbol{y}_{\mathrm{MT}}$, the state matrix $\mathbf{A}_{\mathrm{MT}}$, the input vector $\boldsymbol{b}_{\mathrm{MT}}$ and the output matrix $\mathbf{C}_{\mathrm{MT}}$ of the machine tool, the state-space model is defined as follows:

$$\begin{aligned} \dot{\boldsymbol{x}}_{\mathrm{MT}} &= \mathbf{A}_{\mathrm{MT}}\boldsymbol{x}_{\mathrm{MT}} + \boldsymbol{b}_{\mathrm{MT}}u_{\mathrm{MT}} \\ \boldsymbol{y}_{\mathrm{MT}} &= \mathbf{C}_{\mathrm{MT}}\boldsymbol{x}_{\mathrm{MT}} \end{aligned} \tag{D15}$$

with

$$\begin{aligned} \boldsymbol{x}_{\mathrm{MT}} &= \left(p_{\mathrm{f}}\ v_{\mathrm{f}}\ \dot{v}_{\mathrm{f}}\right)^{\mathrm{T}}, \\ u_{\mathrm{MT}} &= v_{\mathrm{f,cmd}}, \\ \boldsymbol{y}_{\mathrm{MT}} &= \left(p_{\mathrm{f}}\ v_{\mathrm{f}}\right)^{\mathrm{T}}. \end{aligned} \tag{D16}$$

The state matrix $\mathbf{A}_{\mathrm{MT}}$, the input vector $\boldsymbol{b}_{\mathrm{MT}}$ and the output matrix $\mathbf{C}_{\mathrm{MT}}$ of the machine tool read

$$\begin{aligned} \mathbf{A}_{\mathrm{MT}} &= \begin{pmatrix} 0 & 1 & 0 \\ 0 & 0 & 1 \\ 0 & -\omega_0^2 & -2\zeta\omega_0 \end{pmatrix}, \\ \boldsymbol{b}_{\mathrm{MT}} &= \left(0\ 0\ K\omega_0^2\right)^T, \\ \mathbf{C}_{\mathrm{MT}} &= \begin{pmatrix} 1 & 0 & 0 \\ 0 & 1 & 0 \end{pmatrix}. \end{aligned} \tag{D17}$$

Since the MPC operates in a discrete manner, the continuous machine model in Eq. (D15) is discretized. Consequently, the state matrix $\mathbf{A}_{\mathrm{MT}}$ and the input vector $\boldsymbol{b}_{\mathrm{MT}}$ are transformed in their discrete forms according to Tsai et al. (2011), denoted as $\mathbf{A}_{\mathrm{MT,D}}$ and $\boldsymbol{b}_{\mathrm{MT,D}}$, respectively. The output matrix $\mathbf{C}_{\mathrm{MT}}$ remains unaffected by the discretization. The resulting discrete state-space reads

$$\begin{aligned} \boldsymbol{x}_{\mathrm{MT}}(k+1) &= \mathbf{A}_{\mathrm{MT,D}}\boldsymbol{x}_{\mathrm{MT}}(k) + \boldsymbol{b}_{\mathrm{MT,D}}u(k - N_{\mathrm{t}} - 1), \\ \boldsymbol{y}_{\mathrm{MT}}(k) &= \mathbf{C}_{\mathrm{MT}}\boldsymbol{x}_{\mathrm{MT}}(k) \end{aligned} \tag{D18}$$

for each time step k. The time delay T_{d} is represented by time delay's number of time steps N_{t} times the sampling time T_{s} according to

$$T_{\mathrm{d}} = N_{\mathrm{t}}T_{\mathrm{s}}. \tag{D19}$$

Due to the system's inherent time delay N_{t}, the control inputs cannot influence the state dynamics between the current time step k and time step $k + N_{\mathrm{t}}$. Consequently, the states are propagated as

$$\boldsymbol{x}_{\mathrm{MT}}(k + N_{\mathrm{t}}|k) = \mathbf{A}_{\mathrm{MT,D}}^{N_{\mathrm{t}}} + \sum_{j=1}^{N_{\mathrm{t}}-1} \mathbf{A}_{\mathrm{MT,D}}^{j-1}\boldsymbol{b}_{\mathrm{MT,D}}v_{\mathrm{f,cmd}}(k-j). \tag{D20}$$

Based on these propagated states, the prediction of the MPC reads

$$\begin{aligned} \boldsymbol{y}_{\mathrm{MT}}(\cdot|k) &= \begin{pmatrix} p_{\mathrm{f}}(k+N_1|k) \\ v_{\mathrm{f}}(k+N_1|k) \\ \vdots \\ p_{\mathrm{f}}(k+N_2|k) \\ v_{\mathrm{f}}(k+N_2|k) \end{pmatrix} \\ &= \begin{pmatrix} \mathbf{C}_{\mathrm{MT}}\mathbf{A}_{\mathrm{MT,D}}^{N_1-N_{\mathrm{t}}} \\ \vdots \\ \mathbf{C}_{\mathrm{MT}}\mathbf{A}_{\mathrm{MT,D}}^{N_2-N_{\mathrm{t}}} \end{pmatrix} \boldsymbol{x}_{\mathrm{MT}}(k+N_{\mathrm{t}}|k) \\ &+ \begin{pmatrix} \mathbf{C}_{\mathrm{MT}}\sum_{j=0}^{N_1-N_{\mathrm{t}}-1}\mathbf{A}_{\mathrm{MT,D}}^{j}\boldsymbol{b}_{\mathrm{MT,D}} \\ \vdots \\ \mathbf{C}_{\mathrm{MT}}\sum_{j=0}^{N_2-N_{\mathrm{t}}-1}\mathbf{A}_{\mathrm{MT,D}}^{j}\boldsymbol{b}_{\mathrm{MT,D}} \end{pmatrix} v_{\mathrm{f,cmd}}(k-1) \\ &+ \begin{pmatrix} \Psi(N_1 - N_{\mathrm{t}} - 1) & \dots & \Psi(N_1 - N_{\mathrm{t}} - N_{\mathrm{u}}) \\ \vdots & \ddots & \vdots \\ \Psi(N_2 - N_{\mathrm{t}} - 1) & \dots & \Psi(N_2 - N_{\mathrm{t}} - N_{\mathrm{u}}) \end{pmatrix} \\ &\Delta\boldsymbol{v}_{\mathrm{f,cmd}}(\cdot|k) \end{aligned} \tag{D21}$$

with

$$\Psi(i) = \begin{cases} \mathbf{C}_{\mathrm{MT}}\sum_{j=0}^{i}\mathbf{A}_{\mathrm{MT,D}}^{j}\boldsymbol{b}_{\mathrm{MT,D}} & , i \geq 1 \\ \mathbf{0} & , i < 1. \end{cases} \tag{D22}$$

Appendix E Details on approximation quality

To evaluate the influence of the sample time on the determined approximation quality, we further examined the difference between the maximum active force predicted by the approximation methods and the maximum active force derived from the sliding window. The simulation model ran with a sampling time of 0.2 ms, which resulted in the simulation of the angular position with an increment of $\Delta\varphi_0 = 0.0533\,\text{rad}$. Since the approximation methods did not account for the sampling rate of the simulation model, a small difference emerged between the predicted angular position $\varphi_{0,\max}$ with the maximum force from the approximation methods and the angular position from the sliding window. This angular difference $\Delta\varphi_{0,\max}$ resulted in an error in the maximum force. To determine the relevance of this effect, we calculated the MAE for all values in the range $[0, \Delta\varphi_{0,\max}]$ exemplarily for three-axis milling with the feed velocity $v_f = 183.35\,\text{mm}\,\text{min}^{-1}$. The result is shown in Fig. 12. The black line indicates the length of an increment in the angular position.

For both AC and AMS, the MAE increased with increasing angular difference, as long as the angular difference is smaller than an increment in the angular position. Thus, the periodic deviation was caused by the sampling time of the simulation model. In three-axis milling, the MAE did not increase substantially after an increment of the angular position was reached. Hence, the approximation methods located the same angular position as the sliding window in nearly every instance, and most of the model error was caused by the sampling rate of the simulation model.

The evaluation also indicates that the influence of the periodic deviation is likely less than 1 N. Consequently, the approximation error in multi-axis milling cannot be attributed solely to this numerical effect.

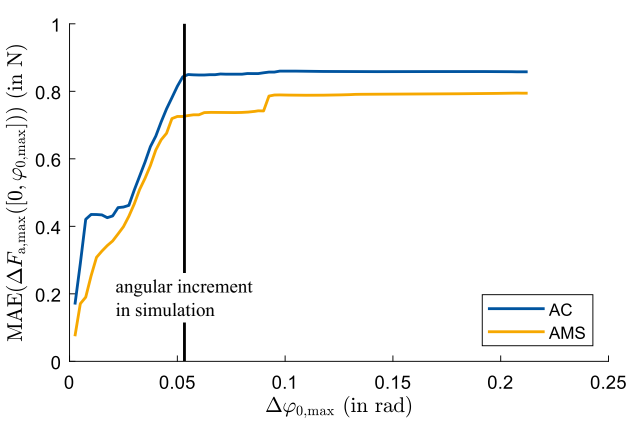

Fig. 12 Dependence of the maximum force difference on the angular position inaccuracy

Author Contributions Conceptualization: Patrick Ochudlo, Adrian Karl Rüppel; Methodology: Patrick Ochudlo, Adrian Karl Rüppel, Lorenz Schmidt; Formal analysis and investigation: Patrick Ochudlo, Adrian Karl Rüppel; Writing - original draft preparation: Patrick Ochudlo; Writing - review and editing: Patrick Ochudlo, Adrian Karl Rüppel, Lorenz Schmidt, Heike Vallery, Sebastian Stemmler; Funding acquisition: Thomas Bergs, Sebastian Stemmler; Resources: Thomas Bergs; Supervision: Thomas Bergs, Heike Vallery, Sebastian Stemmler

Funding Open Access funding enabled and organized by Projekt DEAL. The presented research was funded by the Deutsche Forschungsgemeinschaft (DFG, German Research Foundation)—450794086.

Data Availability The measurement data is freely available in the accompanying data publication (Ochudlo et al., 2026).

Declarations

Ethics approval and consent to participate Not applicable

Consent for publication Not applicable

Materials availability Not applicable

Code availability Not applicable

Competing interests The authors have no relevant financial or non-financial interests to disclose.

References

Altintas, Y. (1994). Direct adaptive control of end milling process. *International Journal of Machine Tools and Manufacture, 34*(4), 461–472. https://doi.org/10.1016/0890-6955(94)90078-7

Altintas, Y., Kersting, P., Biermann, D., Budak, E., Denkena, B., & Lazoglu, I. (2014). Virtual process systems for part machining operations. *CIRP Annals, 63*(2), 585–605. https://doi.org/10.1016/j.cirp.2014.05.007

Altintas, Y., Kersting, P., Biermann, D., Budak, E., Denkena, B., & Lazoglu, I. (2014). Virtual process systems for part machining operations. *CIRP Annals, 63*(2), 585–605. https://doi.org/10.1016/j.cirp.2014.05.007

Altintas, Y., & Munasinghe, W. K. (1996). Modular CNC design for intelligent machining, part 2: Modular integration of sensor based milling process monitoring and control tasks. *Journal of Manufacturing Science and Engineering, 118*, 514–521. https://doi.org/10.1115/1.2831061

Bakhshandeh, P., Mohammadi, Y., Altintas, Y., & Bleicher, F. (2024). Digital twin assisted intelligent machining process monitoring and control. *CIRP Journal of Manufacturing Science and Technology,49*, 180–190. https://doi.org/10.1016/j.cirpj.2024.01.005

Boz, Y., Demir, O., & Lazoglu, I. (2010). Model based feedrate scheduling for free-form surface machining. *International Journal of Automation Technology, 4*(3), 273–283. https://doi.org/10.20965/ijat.2010.p0273

Fussell, B. K., & Srinivasan, K. (1991). Adaptive control of force in end milling operations– an evaluation of available algorithms. *Journal of Manufacturing Systems, 10*(1), 8–20. https://doi.org/10.1016/0278-6125(91)90043-2

Ganser, P., Venek, T., Rudel, V., & Bergs, T. (2021). Dpart - a digital twin framework for the machining domain. *MM Science Journal, 2021*(5), 5134–5141. https://doi.org/10.17973/MMSJ.2021_11_2021168

Jun-Ho Oh, M. (1983). Tomizuka: Model reference adaptive control of the milling process

Erkorkmaz, S., Layegh, E., Lazoglu, I., & Erdim, H. (2013). Feedrate optimization for freeform milling considering constraints from the feed drive system and process mechanics. *CIRP Annals,62*(1), 395–398. https://doi.org/10.1016/j.cirp.2013.03.084

Kienzle, O. (1952). Die bestimmung von kräften und leistungen an spanenden werkzeugmaschinen. In: rVerein Deutscher Ingenieure (ed.) VDI-Z: Zeitschrift Für die Entwicklung, Konstruktion, Produktion, pp. 299–305.

Kline, W. A., DeVor, R. E., & Lindberg, J. R. (1982). The prediction of cutting forces in end milling with application to cornering cuts. *International Journal of Machine Tool Design and Research, 22*(1), 7–22. https://doi.org/10.1016/0020-7357(82)90016-6

Klocke, F. (2011). Manufacturing Processes 1: Cutting. RWTHedition Ser. Springer Berlin / Heidelberg, Berlin, Heidelberg. https://doi.org/10.1007/978-3-642-11979-8

Koren, Y. (1988). Adaptive control systems for machining. In: 1988 American Control Conference, pp. 1161–1167. IEEE, Atlanta. https://doi.org/10.23919/ACC.1988.4789896

Kuljanic, E., Sortino, M., Miani, F. (2002). Application of a rotating dynamometer for cutting force measurement in milling. In: rKulianic, E. (ed.) AMST'02 Advanced Manufacturing Systems and Technology, pp. 159–166. Springer Vienna, Vienna. https://doi.org/10.1007/978-3-7091-2555-7_15

Kurt, M., & Bagci, E. (2011). Feedrate optimisation/scheduling on sculptured surface machining: a comprehensive review, applications and future directions. *The International Journal of Advanced Manufacturing Technology, 55*(9–12), 1037–1067. https://doi.org/10.1007/s00170-010-3131-3

Lauderbaugh, L. K., & Ulsoy, A. G. (1989). Model reference adaptive force control in milling. *Journal of Engineering for Industry, 111*(1), 13–21. https://doi.org/10.1115/1.3188726

Lee, P., & Altintaş, Y. (1996). Prediction of ball-end milling forces from orthogonal cutting data. *International Journal of Machine Tools and Manufacture, 36*(9), 1059–1072. https://doi.org/10.1016/0890-6955(95)00081-X

Liang, S. Y., Hecker, R. L., & Landers, R. G. (2004). Machining process monitoring and control: The state-of-the-art. *Journal of Manufacturing Science and Engineering, 126*(2), 297–310. https://doi.org/10.1115/1.1707035

Liu, Y.-P., Kilic, Z. M., & Altintas, Y. (2022). Monitoring of in-process force coefficients and tool wear. *CIRP Journal of Manufacturing Science and Technology, 38*, 105–119. https://doi.org/10.1016/j.cirpj.2022.04.009

López de Lacalle, L. N., Lamikiz, A., Sánchez, J. A., & Salgado, M. A. (2007). Toolpath selection based on the minimum deflection cutting forces in the programming of complex surfaces milling. *International Journal of Machine Tools and Manufacture, 47*(2), 388–400. https://doi.org/10.1016/j.ijmachtools.2006.03.010

Maciejowski, J. M. (2002). *Predictive Control: with Constraints* (publ, Vol. 1). Harlow and Munich: Prentice Hall.

Matsubara, A., & Ibaraki, S. (2009). Monitoring and control of cutting forces in machining processes: A review. *International Journal of Automation Technology, 3*(4), 445–456. https://doi.org/10.20965/ijat.2009.p0445

Milner, D. A. (1974). Adaptive control of feedrate in the milling process. *International Journal of Machine Tool Design and Research, 14*(2), 187–197. https://doi.org/10.1016/0020-7357(74)90026-2

Möhring, H.-C., Werkle, K., & Maier, W. (2020). Process monitoring with a cyber-physical cutting tool. *Procedia CIRP, 93*, 1466–1471. https://doi.org/10.1016/j.procir.2020.03.034

Nishida, I., Tsuyama, R., Shirase, K., Onishi, M., & Koarashi, K. (2019). Development of innovative intelligent machine tool based on cam-cnc integration concept - adaptive control based on predicted cutting force -. *International Journal of Automation Technology, 13*(3), 373–381. https://doi.org/10.20965/ijat.2019.p0373

Ochudlo, P., Rüppel, A.K., Schmidt, L., Bergs, T., Vallery, H., & Stemmler, S. (2026). Dataset for Model Predictive Force Control in Five-Axis Positional Milling using a Table Dynamometer. https://doi.org/10.18154/RWTH-2026-03847

Ochudlo, P., Rüppel, A.K., Stemmler, S., Bergs, T., & Abel, D. (2023). Model-based determination of process force in multi-axis milling. In: Proceedings of the 9th World Congress on Mechanical, Chemical, and Material Engineering. World Congress on Mechanical, Chemical, and Material Engineering. Avestia Publishing, Orléans, ON, Canada. https://doi.org/10.11159/mmme23.117

Olvera, D., Artetxe, E., Luo, M., & Urbikain, G. (2020). 5-axis milling of complex parts with barrel-shape cutter: cutting force model and experimental validation. *Procedia Manufacturing, 48*, 528–532. https://doi.org/10.1016/j.promfg.2020.05.079

Powell, M. (2009). The bobyqa algorithm for bound constrained optimization without derivatives

Rüppel, A. K., Ochudlo, P., Bickel, M., Stemmler, S., Bergs, T., & Abel, D. (2023). Mass loss and displacement modeling for multi-axis milling. *Procedia CIRP, 120*, 1534–1539. https://doi.org/10.1016/j.procir.2023.09.210

Rüppel, A. K., Ochudlo, P., Meurer, M., Bergs, T., & Stemmler, S. (2024). Dynamic process force simulation model for multi-axis milling processes. *IFAC-PapersOnLine, 58*(19), 1078–1083. https://doi.org/10.1016/j.ifacol.2024.09.128

Salami, R., Sadeghi, M. H., & Motakef, B. (2007). Feed rate optimization for 3-axis ball-end milling of sculptured surfaces. *International Journal of Machine Tools and Manufacture, 47*(5), 760–767. https://doi.org/10.1016/j.ijmachtools.2006.09.011

Schmid, C., & Biegler, L. T. (1994). Quadratic programming methods for reduced hessian sqp. *Computers & Chemical Engineering, 18*(9), 817–832. https://doi.org/10.1016/0098-1354(94)E0001-4

Schuster, A., Rentzsch, H., & Ihlenfeldt, S. (2023). Energy self-sufficient, multi-sensory tool holder for sensitive monitoring of milling processes. *Procedia CIRP, 117*, 80–85. https://doi.org/10.1016/j.procir.2023.03.015

Schwenzer, M. (2022). Closing the Loop of Model Predictive Force Control in Milling with Ensemble Kalman Filtering, 1. auflage edn. Ergebnisse aus der Produktionstechnik, vol. 13/2022. Apprimus Verlag, Aachen

Schwenzer, M., Stemmler, S., Ay, M., Rüppel, A. K., Bergs, T., & Abel, D. (2022). Model predictive force control in milling based on an ensemble kalman filter. *Journal of Intelligent Manufacturing, 33*(7), 1907–1919. https://doi.org/10.1007/s10845-022-01931-2

Seco Tools GmbH: JS553030G2R050.0Z3-SIRA | Seco Tools (2025). www.secotools.com/article/p_10052995?language=en Accessed 02.01.2025

Smith, S., McFarland, J., Assaid, T., Tursky, D., Barkman, W., & Babelay, E. (2010). Surface characteristics generated in cnc chip breaking tool paths. *CIRP Annals, 59*(1), 137–140. https://doi.org/10.1016/j.cirp.2010.03.060

Stemmler, S. (2020). Intelligent control strategies as an enabler for self-optimizing manufacturing systems. PhD thesis, RWTH Aachen University. https://doi.org/10.18154/RWTH-2020-02766

Stemmler, S., Ay, M., Schwenzer, M., Abel, D., & Bergs, T. (2019). Model-based predictive force control in milling. In: 2019 18th European Control Conference (ECC), pp. 4313–4318. IEEE, Piscataway, NJ. https://doi.org/10.23919/ECC.2019.8795716

Stemmler, S., Abel, D., Schwenzer, M., Adams, O., & Klocke, F. (2017). Model predictive control for force control in milling. *IFAC-PapersOnLine, 50*(1), 15871–15876. https://doi.org/10.1016/j.ifacol.2017.08.2336

Sutherland, J. W., & DeVor, R. E. (1986). An improved method for cutting force and surface error prediction in flexible end milling systems. *Journal of Engineering for Industry, 108*(4), 269–279. https://doi.org/10.1115/1.3187077

Tong, X., Liu, Q., Zhou, Y., & Sun, P. (2023). A digital twin-driven cutting force adaptive control approach for milling process. *Journal of Intelligent Manufacturing, 36*(1), 551–568. https://doi.org/10.1007/s10845-023-02193-2

Tsai, J.S.-H., Huang, C.-C., Guo, S.-M., & Shieh, L.-S. (2011). Continuous to discrete model conversion for the system with a singular system matrix based on matrix sign function. *Applied Mathematical Modelling, 35*(8), 3893–3904. https://doi.org/10.1016/j.apm.2011.02.009

Ulsoy, A. G., & Koren, Y. (1989). Applications of adaptive control to machine tool process control. *IEEE Control Systems Magazine, 9*(4), 33–37. https://doi.org/10.1109/37.24837

Ulsoy, A. G., & Koren, Y. (1993). Control of machining processes. *Journal of Dynamic Systems, Measurement, and Control,115*(2B), 301–308. https://doi.org/10.1115/1.2899070

Zuperl, U., & Cus, F. (2012). System for off-line feedrate optimization and neural force control in end milling. *International Journal of Adaptive Control and Signal Processing,26*(2), 105–123. https://doi.org/10.1002/acs.1277